



Dual-energy computed tomography could reliably differentiate metastatic from non-metastatic lymph nodes of less than 0.5 cm in patients with papillary thyroid carcinoma

Ying Zou^{1,2#}, Meizhu Zheng^{3#}, Ziyu Qi¹, Yu Guo⁴, Xiaodong Ji⁴, Lixiang Huang⁴, Yan Gong^{1,5}, Xiudi Lu^{1,2}, Guolin Ma^{6*}, Shuang Xia^{4*}

¹Radiological Department, First Central Clinical College, Tianjin Medical University, Tianjin, China; ²Radiological Department, First Teaching Hospital of Tianjin University of Traditional Chinese Medicine, Tianjin, China; ³Radiological Department, Third Central Hospital of Tianjin, Tianjin, China; ⁴Department of Radiology, Tianjin First Central Hospital, School of Medicine, Nankai University, Tianjin, China; ⁵Radiological Department, Tianjin Hospital of ITCWM Nankai Hospital, Tianjin, China; ⁶Radiological Department, China-Japan Friendship Hospital, Beijing, China

#These authors contributed equally to this work.

*These authors contributed equally to this work as co-corresponding authors.

Correspondence to: Shuang Xia, MD, PhD. 24 Fukang Road, Nankai District, Department of Radiology, Tianjin First Central Hospital, School of Medicine, Nankai University, Tianjin 300192, China. Email: xiashuang77@163.com; Guolin Ma, MD, PhD. Yinghuayuan East Street, Chao Yang District, Beijing, China. Email: maguolin1007@qq.com.

Background: Dual-energy computed tomography (DECT) has been widely applied to detect lymph node (LN) and lymph node metastasis (LNM) in various cancers, including papillary thyroid carcinoma (PTC). This study aimed to quantitatively evaluate metastatic cervical lymph nodes (LNs) <0.5 cm in patients with PTC using DECT, which has not been done in previous studies.

Methods: Preoperative DECT data of patients with pathologically confirmed PTC were retrospectively collected and analyzed between May 2016 and June 2018. A total of 359 LNs from 52 patients were included. Diameter, iodine concentration (IC), normalized iodine concentration (NIC), and the slope of the energy spectrum curve (λ_{HU}) of LNs in the arterial and the venous phases were compared between metastatic and non-metastatic LNs. The optimal parameters were obtained from the receiver operating characteristic (ROC) curves. The generalized estimation equation (GEE) model was used to evaluate independent diagnostic factors for LNM.

Results: A total of 139 metastatic and 220 non-metastatic LNs were analyzed. There were statistical differences of quantitative parameters between the two groups (P value 0.000–0.007). The optimal parameter for diagnosing LNM was IC in the arterial phase, and its area under the curve (AUC), sensitivity, and specificity were 0.775, 71.9%, and 73.6%, respectively. When the three parameters of diameter, IC in the arterial phase, and NIC in the venous phase were combined, the prediction efficiency was better, and the AUC was 0.819. The GEE results showed that LNs located in level VIa [odds ratio (OR) 2.030, 95% confidence interval (CI): 1.134–3.634, P=0.017], VIb (OR 2.836, 95% CI: 1.597–5.038, P=0.000), diameter (OR 2.023, 95% CI: 1.158–3.532, P=0.013), IC in the arterial phase (OR 4.444, 95% CI: 2.808–7.035, P=0.000), and IC in the venous phase (OR 5.387, 95% CI: 3.449–8.413, P=0.000) were independent risk factors for LNM in patients with PTC.

Conclusions: DECT had good diagnostic performance in the differentiation of cervical metastatic LNs <0.5 cm in patients with PTC.

Keywords: Papillary thyroid carcinoma (PTC); lymph nodes (LNs); metastasis; dual-energy computed tomography (DECT); iodine concentration (IC)

Submitted Jul 08, 2020. Accepted for publication Nov 09, 2020.

doi: 10.21037/qims-20-846

View this article at: <http://dx.doi.org/10.21037/qims-20-846>

Introduction

Cervical lymph node (LN) and lymph node metastasis (LNM) is extremely common in patients with papillary thyroid carcinoma (PTC), with an incidence of 30–80% (1,2). Lymph nodes (LNs) with a short diameter of >0.5 cm can be easily detected by computed tomography (CT) (3), especially when the diameter is >1 cm. However, according to current literature, the detection of LNs <0.5 cm using traditional examination methods is challenging. The risk of recurrence of LNM varies from 4% with metastatic LNs <0.2 cm to 27–32% with metastatic LNs >3 cm (4,5). A large, population-based study showed that there was an association between the metastatic LN ratio and disease-specific mortality in 60–75% of patients with PTC (6). After LN dissection, the 5-year survival rate can reach 100%, and the 20-year survival rate can exceed 90% (7). Therefore, the treatment regimen is influenced by whether metastatic LNs are present or absent (8).

According to the American Thyroid Association (ATA) statement on preoperative imaging for thyroid cancer surgery, ultrasound (US) stands as the key imaging modality for the assessment of thyroid cancer (9); however, US can only detect 20–31% of patients with central cervical LNM (10–13), whereas the rate of detection for lateral cervical LNM is 70–93.8% (11,12). US is also greatly affected by the operators' experience level and manipulation (14–16). For PTC patients, the spatial resolution and contrast resolution of traditional CT scans are not high enough for cervical LNs to be accurately detected, as these LNs cannot be easily distinguished from accompanying blood vessels, especially when they measure <0.5 cm (17,18). Diffusion weighted imaging (DWI) has high diagnostic value for distinguishing metastatic and non-metastatic LNs, with an accuracy rate of 91.0–94.3% (19). However, the apparent diffusion coefficient (ADC) value does not apply to cystic degeneration and necrosis in LNs (20–22), especially in the investigation of LNs with a diameter <0.5 cm.

In recent years, dual-energy computed tomography (DECT) has been widely used in the prediction of numerous diseases, such as adherent perinephric fat (23), microthrombosis associated with COVID-19 pneumonia (24), detection of pulmonary emboli (25), and detection of lumbar disk herniation (26). Besides, DECT has been used to predict LNM in some cancers, including lung cancer (19), gastrointestinal tumor (27), breast cancer (28), biliary tract cancer (29), and hepatocellular carcinoma (30). According to the Chinese Society of Clinical Oncology (CSCO) diagnosis

and treatment guidelines for persistent/recurrent and metastatic differentiated thyroid cancer (version 2018) (31), when there are suspected local lesions, neck US, enhanced CT, or contrast magnetic resonance imaging (MRI) are juxtaposed as a level I–2A recommendation, which is the highest recommendation. Additionally, in the National Comprehensive Cancer Network (NCCN) guidelines (version 2018), for papillary carcinoma or suspicion of papillary carcinoma, the use of CT/MRI with contrast was suggested for fixed, bulky, or substernal lesions. This supports the idea that enhanced CT is not a contraindication for patients with PTC. Moreover, CT examination can more accurately determine the extent of LNM, thus playing a vital role in the planning of surgical procedures. Details on the specific reasons for applying DECT in the current study are displayed in [Appendix 1](#). However, there may be concerns regarding the use of iodinated contrast agents, which can compete with iodine-131 (^{131}I) and interfere with subsequent postoperative radioactive iodine (RAI) therapy. In fact, a potential delay in RAI treatment is not harmful, for the reasons detailed in [Appendix 1](#). Meanwhile, DECT can not only obtain more parameters than ordinary enhanced CT, but it also has a significantly lower radiation dose, which has been verified in previous studies (32,33). A study conducted by Liu *et al.* suggested that the slope of the energy spectrum curve (λ_{HU}) in the venous phase and the normalized iodine concentration (NIC) in the arterial phase are effective parameters for diagnosing LNM in patients with PTC (33). However, to date, no relevant studies on metastatic or non-metastatic LNs with a short diameter of <0.5 cm in patients with PTC have been performed.

In the current study, we hypothesized that DECT could distinguish metastatic LNs from non-metastatic LNs with a short diameter <0.5 cm in patients with PTC. Therefore, the main purpose of this study was to investigate the usefulness of quantitative DECT parameters in the preoperative diagnosis of cervical small LNM in patients with PTC.

Methods

Patient population

This retrospective study was approved by the ethics committee of the Tianjin First Central Hospital (2018N131KY), and the requirement for written informed consent was waived due to its retrospective nature. Between May 2016 and June 2018, 165 patients (29 male, mean age,

48.97±17.30 years; 136 female, mean age, 49.48±12.41 years) suspected as thyroid carcinoma by US were initially consecutively selected. The patients underwent DECT to rule out or confirm the presence of metastatic LNs (according to the CSCO guidelines, version 2018) (31). The inclusion criteria were: (I) >18 years old; (II) PTC confirmed by postoperative pathology; and (III) no history of radiotherapy to the neck. The investigated LNs with a short diameter <0.5 cm was included for further analysis. Other inclusion criteria are listed in [Appendix 1](#). The exclusion criteria included: (I) patients who did not receive surgical treatment; (II) patients whose postoperative pathology confirmed a nodular goiter, adenoma, thyroiditis, or other benign lesion; (III) patients whose pathology confirmed medullary thyroid carcinoma (MTC) or follicular thyroid cancer (FTC); (IV) patients with incomplete information, and (V) patients with history of neck cancer other than PTC (i.e., pharyngeal carcinoma, neck squamous cell carcinoma, and nasopharyngeal carcinoma). Eventually, 52 patients comprising 11 males (mean age, 43.00±15.22 years) and 41 females (mean age, 44.68±10.36 years) were included. The detailed inclusion and exclusion criteria are shown in [Figure S1](#).

The shortest diameter of the largest layer of a LN and quantitative parameters, including iodine concentration (IC), NIC, and λ_{HU} in the arterial and the venous phases, which was derived from DECT, were measured for all of the LNs of the enrolled participants. Distinct from the experimental method of Liu *et al.* (33), our study referred to Park's method (34) to solve the problems of LNs between the pathological results and DECT. The final histopathologic reports of the surgical neck dissection samples served as the gold standard for LNM. All cervical levels in a neck dissection specimen were labeled based on the newest cervical LN partition standard (35), which was published by the official journal of the European Society of Radiotherapy & Oncology (ESTRO)-Radiotherapy & Oncology (Green Skin Magazine) in November 2013. Cervical LN levels were assigned as non-metastatic, metastatic, or mixed after correlation with the histopathologic reports. If pathological results showed metastasis in all LNs in a subregion, the level was classified as metastatic. If the pathological results showed no metastasis in any of the LNs in a subregion, the level was classified as non-metastatic. If both benign and metastatic LNs were found in a subregion, the level was classified as mixed. The levels with mixed LNs were ruled out, and only levels with non-metastatic or metastatic LNs were

included, regardless of the diameter of the LNs. Finally, only LNs with a diameter <0.5 cm measured by DECT were included, and LNs ≥0.5 cm were excluded ([Figures S2,S3](#)). Subsequently, the results of the histopathologic assignment were used to match and label LNs on DECT. An LN confirmed by ultrasound-fine needle aspiration biopsy (US-FNAB) was chosen and labeled on DECT images by matching the images and reports of DECT, US, and the final pathologic examination (site-specific matching, 23 LNs). The LNs were assigned as non-metastatic or metastatic according to the postoperative pathological results and labeled as surgical-level matching (336 LNs). LNs with a diameter ≥0.5 cm and those obscured due to artifacts on the iodine map were also excluded ([Figure 1](#)). The specific lesion measurement method is presented in the supplementary material as legends ([Figures S4,S5,S6](#)). The specific DECT diagnostic criteria of LNM <0.5 cm in patients with PTC are detailed in [Appendix 1](#) and [Figure S7](#).

Image acquisition, processing, and analyzing

All images were obtained using a 64 multi-detector row CT scanner (Somatom Definition Flash, Siemens Healthcare, Forchheim, Germany) with dual-phase contrast-enhanced CT. The detailed CT protocol is provided in [Appendix 1](#).

Region of interest (ROI) segmentation and consistency analysis

All of the LNs were evaluated by two radiologists with proficiency in head and neck disease and 13 and 15 years of experience, respectively. The two radiologists were blinded to one another and the final diagnosis. Each ROI from three different adjacent slices of the neck was drawn to measure the IC of each LN. The ROI was placed in the solid part with an area >2 mm² including the entire LNs ([Figure 2](#)). The criteria for ROI selection are detailed in [Appendix 1](#). The average value from three measurements was taken for final evaluation. An ROI with an area of 20 mm² was drawn on the ipsilateral common carotid artery (CCA) as a reference. One week later, SPSS software version 22.0 (SPSS Inc., IBM Corp., Chicago, IL, USA) was used to randomly select case samples; 14% of data was randomly selected, and 50 LNs were retested. Intra- and inter-observer consistency analyses were performed to confirm the measurement consistency. The measured parameters included the maximal short axial diameter of the LNs, IC of the LNs, and the CCA in the arterial and the

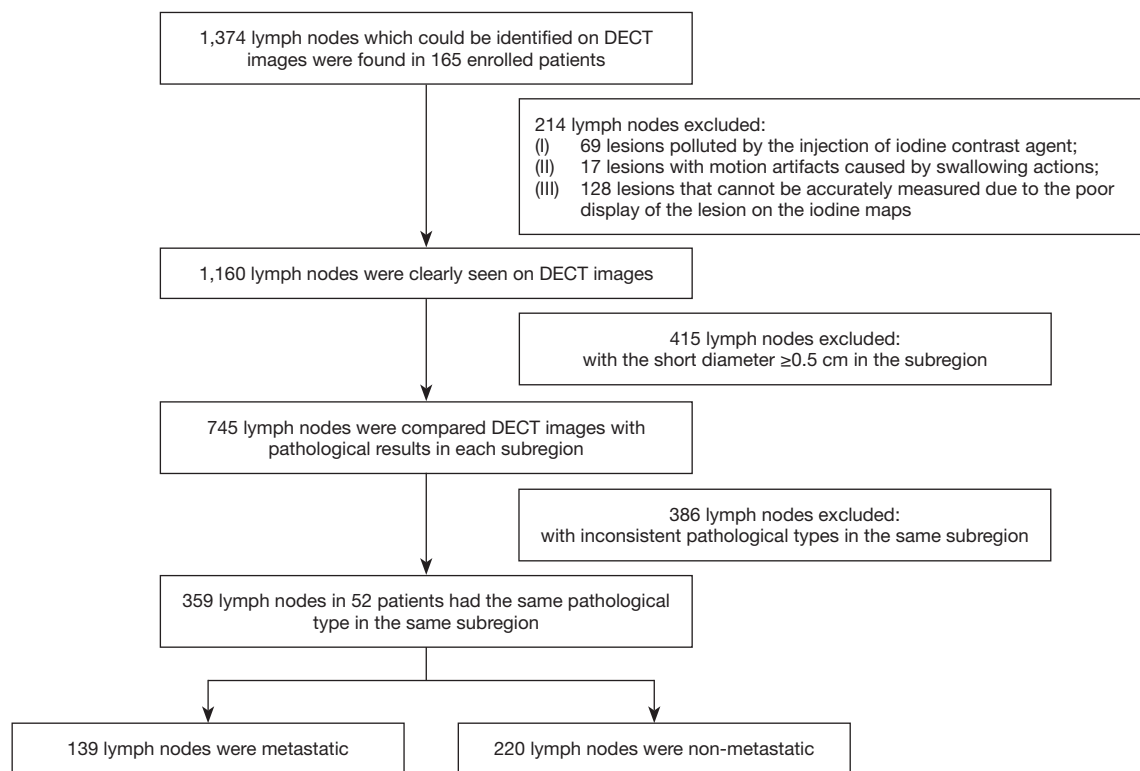


Figure 1 Flowchart showing the inclusion and exclusion criteria of lymph nodes in patients with PTC in the current study. DECT, dual-energy computed tomography; PTC, papillary thyroid carcinoma.

venous phases. The NIC was obtained using the following formula: $NIC = IC_{LN}/IC_{CCA}$. The “Mono Energetic” program was selected for energy spectrum analysis, the energy spectrum Hounsfield Unit (HU), which was defined as the difference between the CT value at 100 keV and that at 140 keV, was calculated as follows: $\lambda_{HU} = (HU_{100\text{ keV}} - HU_{140\text{ keV}})/40$, where HU 100 keV stood for the CT value measured on 100 keV images and HU 140 keV represented the CT value measured on 140 keV images.

Statistical analysis

The IBM software SPSS statistics version 22.0 was used for statistical analysis, and GraphPad prism version 7.04 (GraphPad software, San Diego, CA, USA) and MedCalc version 18.2.1 (MedCalc Software Ltd., Ostend, Belgium) were used to draw graphs. A consistency test was performed to test the agreement of quantitative parameters between the two readers. An intraclass correlation coefficient (ICC) of <0.4 showed a diagnostic test to have poor consistency, while a diagnostic test with an ICC value of >0.75 was considered

to have good consistency. The Kolmogorov-Smirnov (K-S) test method was used to test for the normal distribution of continuous variables of quantitative parameters. If the quantitative parameter fitted the normal distribution, mean \pm standard deviation was used to describe it and t -test was used to compare the difference between metastatic and non-metastatic LNs. If it did not fit the normal distribution, the median (range) and Mann-Whitney U tests were used. The diagnostic ability of the short diameter and quantitative parameters were evaluated by receiver operating characteristic (ROC) curve analysis, and the optimal threshold was selected using the Youden index method. The area under the curve (AUC) of parameters was compared using the z -test. According to the current study design, multiple LNs of the same patient were measured, which could have resulted in a problem with correlation that introduced bias to estimates. To control for this potential issue, a generalized estimating equation (GEE) model with log links with robust variance was used to examine the association of the selected variables with LNM. This statistical method accounted for the correlation between the repeated measures within a

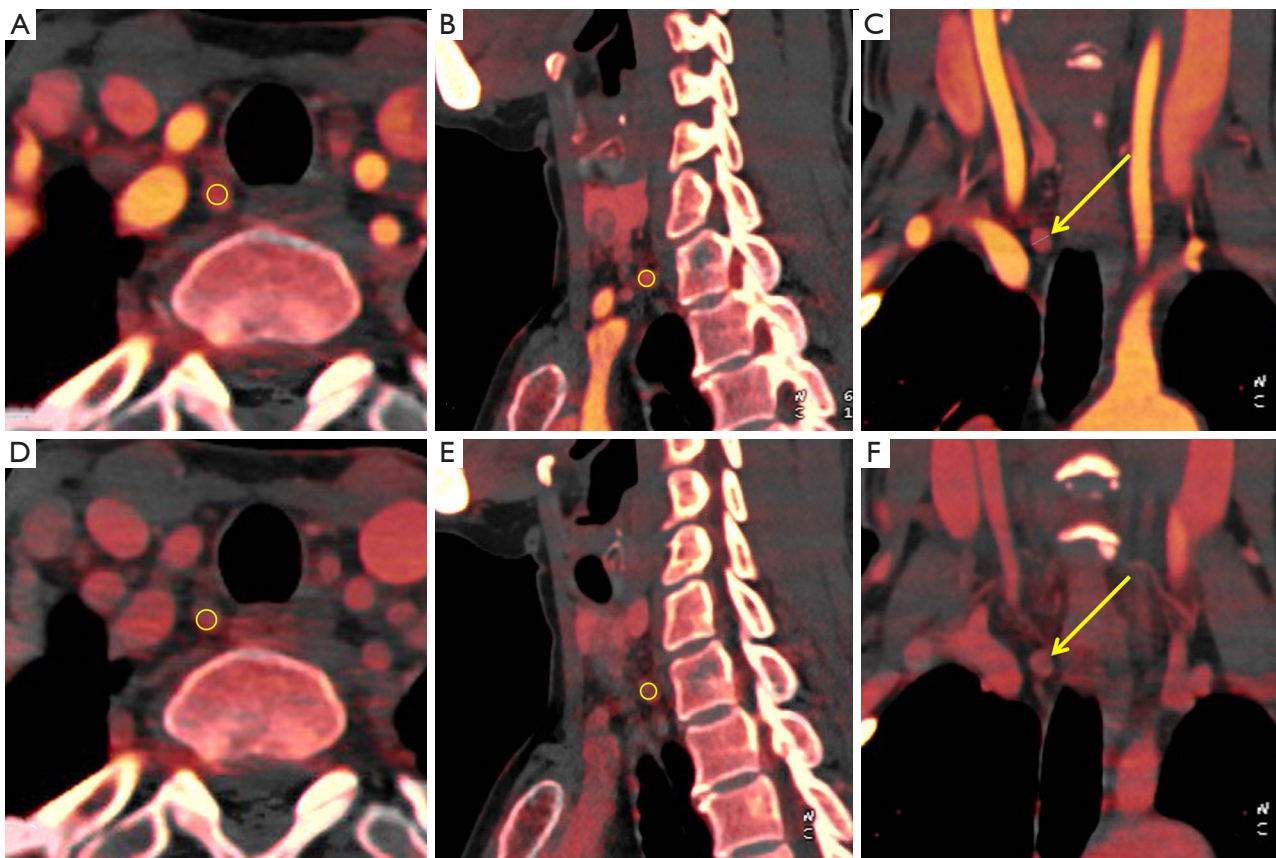


Figure 2 A patient with PTC of the right lobe was confirmed by postoperative pathology, with metastatic lymph nodes in the right level VIb (3/3). (A,B,C) Iodine maps in the arterial phase. An ovoid region of interest (yellow; area, 9 mm^2) was placed on the solid part in combined axial (A), sagittal (B), and coronal (C) images, including the entire lymph node as large as possible, and avoiding peripheral fat, cystic, necrosis, and calcification. (D,E,F) Iodine maps in the venous phase. The short diameter was 0.4 cm. In this case, the iodine concentration was 6.5 mg/mL in the arterial phase and 4.7 mg/mL in the venous phase. PTC, papillary thyroid carcinoma

participant. The GEE parameter estimates were expressed as the coefficients (β), odds ratio (OR), and the 95% confidence intervals (CIs). The multicollinearity of the multivariate model was assessed using the tolerance and variance inflation factor. The test level was set at $P=0.05$.

Results

General information

The demographic, clinical, and pathological characteristics of the 52 patients included in this study are shown in [Table S1](#). A total of 1,374 LNs distributed in all the subregions could be identified on the DECT images of the enrolled patients. A total of 1,160 (87.9%) LNs were seen on DECT without artifacts. Among them, the DECT images

of 745 (64.2%) LNs with a short diameter $<0.5 \text{ cm}$ and pathological results in each level were compared. Finally, a total of 359 (27.2%) small LNs including 139 metastatic and 220 non-metastatic LNs from 52 patients were included and analyzed according to the pathological results after LN dissection. All 359 LNs were located in level II, III, IV, V, VIa, and VIb, respectively. Detailed clinical information of the LNs is shown in [Table 1](#) and [Table S2, Appendix 1](#), and [Figures S8,S9](#).

Result of consistency analysis

The imaging characteristics of DECT were basically consistent between the two radiologists. The inter-observer and intra-observer consistency analysis for all the parameters was >0.75 , which equated to good consistency

(Appendix 1, Table S3 and Figure S10).

Comparison of imaging parameters between metastatic and non-metastatic LNs

The quantitative parameters of metastatic and non-metastatic LNs are listed in Table 2. The diameter, IC in the arterial phase, NIC in the arterial phase, λ_{HU} in the arterial phase, IC in the venous phase, NIC in the venous phase, and λ_{HU} in the venous phase of metastatic LNs were increased compared to those of non-metastatic LNs ($P=0.000-0.007$) (Table 2, Figure 3).

Prediction of each parameter for LNM in patients with PTC

The IC in the arterial phase had the highest AUC (0.775),

Table 1 The different levels between metastatic and non-metastatic LNs

Characteristic	Metastatic LNs, n (%)	Non-metastatic LNs, n (%)	P value
No. of LNs	139	220	–
Levels			0.000
II	13 (9.4)	44 (20.0)	
III	9 (6.5)	42 (19.1)	
IV	15 (10.8)	22 (10.0)	
V	24 (17.3)	17 (7.7)	
VIa	52 (37.4)	89 (40.5)	
VIb	26 (18.7)	6 (2.7)	

LNs, lymph nodes.

Table 2 Comparison of imaging parameters between metastatic and non-metastatic LNs

Parameters	Metastatic LNs	Non-metastatic LNs	Statistics	P value
Diameter (cm)	0.33 (0.14–0.45)	0.30 (0.12–0.45)	12706.5	0.007 [†]
IC IAP (mg/mL)	2.5 (0.4–6.7)	1.65 (0.1–3.9)	6874	0.000 [†]
NIC IAP	0.21 (0.04–0.74)	0.13 (0.01–0.36)	7335	0.000 [†]
λ_{HU} IAP	0.79 (0.05–2.2)	0.6 (0.03–1.55)	7534	0.000 [†]
IC IVP (mg/mL)	2.7 (0.2–6.3)	1.8 (0.1–5.6)	8365	0.000 [†]
NIC IVP	0.56±0.17	0.40±0.19	8.318	0.000 [†]
λ_{HU} IVP	0.83 (0.03–2.3)	0.7 (0.03–3.33)	10,431.5	0.000 [†]

[†], Mann-Whitney U test; [‡], *t*-test. LNs, lymph nodes; IC, iodine concentration; IAP, in the arterial phase; NIC, normalized iodine concentration; λ_{HU} , the slope of energy spectrum curve; IVP, in the venous phase.

with a sensitivity, specificity, and accuracy of 73.63%, 71.94%, and 72.59%, respectively. The cut-off value of each quantitative parameter was obtained (Table 3, Figure 4, Figures S11,S12). The differences among the AUC of quantitative parameters are listed in Table S4. The parameters including IC in the arterial phase *vs.* λ_{HU} in the arterial phase (95% CI: 0.042–0.153; $P=0.0006$), IC in the arterial phase *vs.* λ_{HU} in the venous phase (95% CI: 0.0934–0.237; $P<0.0001$), IC in the venous phase *vs.* λ_{HU} in the arterial phase (95% CI: 0.00766–0.144; $P=0.0292$), IC in the venous phase *vs.* λ_{HU} in the venous phase (95% CI: 0.0854–0.201; $P<0.0001$), NIC in the arterial phase *vs.* λ_{HU} in the arterial phase (95% CI: 0.0215–0.143; $P=0.008$), NIC in the arterial phase *vs.* λ_{HU} in the venous phase (95% CI: 0.0745–0.225; $P=0.0001$), NIC in the venous phase *vs.* λ_{HU} in the arterial phase (95% CI: 0.00347–0.143; $P=0.0396$), NIC in the venous phase *vs.* λ_{HU} in the venous phase (95% CI: 0.0753–0.206; $P<0.0001$), and λ_{HU} in the arterial phase *vs.* λ_{HU} in the venous phase (95% CI: 0.00629–0.129; $P=0.0307$) all showed statistical significance for differentiation between metastatic and non-metastatic LNs.

After binary classification logistic regression model analysis, three parameters including diameter, IC in the arterial phase, and NIC in the venous phase were finally included. In other words, the combination of these three parameters was more effective than using any one parameter alone for the prediction of LNM, with an AUC, sensitivity, and specificity were 0.819, 74.10%, and 77.27%, respectively (Table 4, Figure S13).

GEE estimation of risk factors associated with LNM

Univariable regression analysis showed that level VIa or

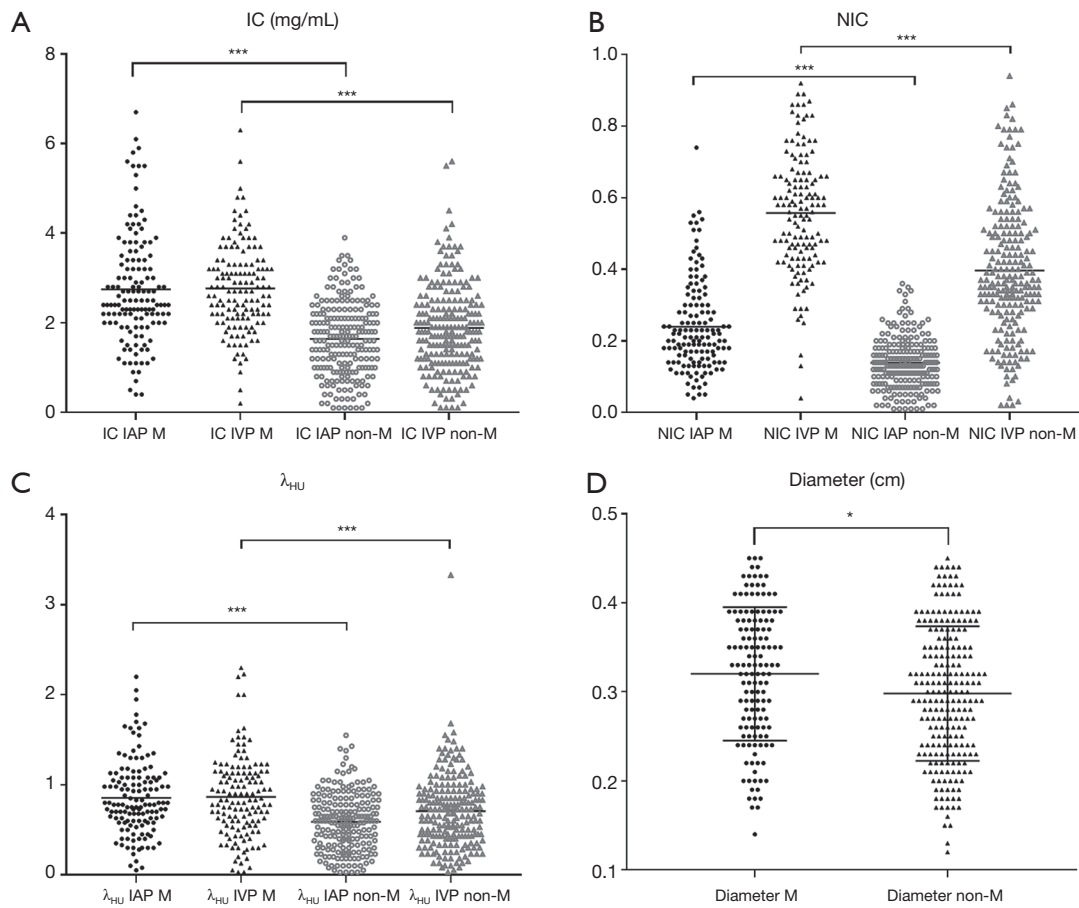


Figure 3 Box plots showing that IC in the arterial and the venous phases (A), NIC in the arterial and the venous phases (B), λ_{HU} in the arterial and the venous phases (C), and diameter (D) had statistical significance in the prediction of metastatic and non-metastatic lymph nodes. *, $P < 0.05$; **, $P < 0.002$; ***, $P < 0.001$. IC, iodine concentration; IAP, in the arterial phase; M, metastasis; IVP, in the venous phase; NIC, normalized iodine concentration; λ_{HU} , the slope of energy spectrum curve.

Table 3 Prediction of each parameter for LNM in patients with PTC

Parameters	Cut-off value	AUC (95% CI)	0.700	P value
Diameter (cm)	0.32	0.584 (0.532–0.636)	—●—	0.0062
IC IAP (mg/mL)	2.1	0.775 (0.728–0.817)	—●—	<0.0001
NIC IAP	0.17	0.760 (0.713–0.803)	—●—	<0.0001
λ_{HU} IAP	0.65	0.693 (0.641–0.741)	—●—	<0.0001
IC IVP (mg/mL)	2.4	0.753 (0.705–0.797)	—●—	<0.0001
NIC IVP	0.40	0.751 (0.703–0.795)	—●—	<0.0001
λ_{HU} IVP	1.00	0.609 (0.556–0.661)	—●—	<0.0001

LNM, lymph node metastasis; PTC, papillary thyroid carcinoma; AUC, area under the curve; IC, iodine concentration; IAP, in the arterial phase; NIC, normalized iodine concentration; λ_{HU} , the slope of the energy spectrum curve; IVP, in the venous phase.

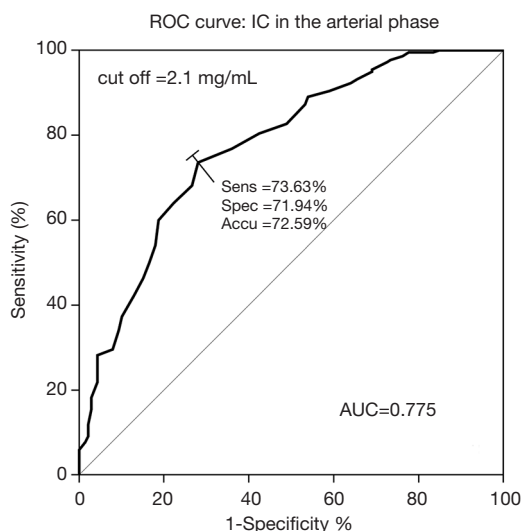


Figure 4 The ROC curve of IC in the arterial phase was used to identify metastatic and non-metastatic lymph nodes. When the cut-off value was 2.1 mg/mL, the sensitivity, specificity, and accuracy were 73.63%, 71.94%, and 72.59%, respectively. ROC, receiver operating characteristic; IC, iodine concentration; AUC, area under the curve.

VIb, diameter, IC in the arterial phase, IC in the venous phase, and λ_{HU} in the venous phase were predictors for predicting LNM ($P=0.000-0.010$). Further multivariable GEE analysis suggested that among these quantitative parameters, LNs being located in level VIa (OR 2.030, 95% CI: 1.134–3.634, $P=0.017$) or VIb (OR 2.836, 95% CI: 1.597–5.038, $P=0.000$), diameter (OR 2.023, 95% CI: 1.158–3.532, $P=0.013$), IC in the arterial phase (OR 4.444, 95% CI: 2.808–7.035, $P=0.000$), and IC in the venous phase (OR 5.387, 95% CI: 3.449–8.413, $P=0.000$) were independent predictors of LNM with a diameter <0.5 cm in patients with PTC. The results of the GEE are shown in *Table 5* and two typical examples are shown in *Figures 5,6*.

The variance inflation factor of each predictor was <10 , and the corresponding tolerance was >0.1 ; therefore, no multicollinearity among these predictors was noted (*Table S5*).

Discussion

In the current study, we found that the DECT quantitative parameters, especially the combination of diameter, IC

Table 4 Prediction of joint parameter for LNM in patients with PTC

Step	B	S.E.	Wald	df	Sig.	Exp (B)
Step 1a						
IC IAP	1.114	0.151	54.601	1	0.000	3.046
Constant	-2.827	0.348	66.120	1	0.000	0.059
Step 1b						
IC IAP	0.919	0.155	35.376	1	0.000	2.508
NIC IVP	4.015	0.812	24.420	1	0.000	55.403
Constant	-4.336	0.503	74.199	1	0.000	0.013
Step 1c						
Diameter	3.943	1.819	4.699	1	0.030	51.565
IC IAP	0.911	0.155	34.343	1	0.000	2.486
NIC IVP	4.028	0.826	23.751	1	0.000	56.141
Constant	-5.555	0.784	50.190	1	0.000	0.004

Variable(s) entered on step 1: IC IAP; variable(s) entered on step 2: NIC IVP; variable(s) entered on step 3: diameter. LNM, lymph node metastasis; PTC, papillary thyroid carcinoma; IC, iodine concentration; IAP, in the arterial phase; NIC, normalized iodine concentration; IVP, in the venous phase.

Table 5 Multivariate analysis for associations between DECT parameters and LNM performed by GEE

Parameters	β	S.E.	Wald χ^2	OR	95% CI	P value
Univariate analysis						
Level						
II	0 [*]	N/A	N/A	1	N/A	N/A
III	-0.033	0.1869	0.031	0.968	0.671–1.396	0.861
IV	0.384	0.2246	2.923	1.468	0.945–2.280	0.087
V	0.416	0.2622	2.512	1.515	0.906–2.534	0.113
VIa	0.840	0.2166	15.029	2.316	1.515–3.541	0.000
VIb	1.057	0.2610	16.411	2.878	1.726–4.800	0.000
Diameter (cm) ≥ 0.32	0.683	0.2648	6.650	1.979	1.178–3.326	0.010
IC IAP (mg/mL) ≥ 2.1	1.489	0.2171	47.030	4.433	2.897–6.785	0.000
NIC IAP ≥ 0.17	-0.048	0.1289	0.140	0.953	0.740–1.227	0.709
λ_{HU} IAP ≥ 0.65	0.044	0.1308	0.113	1.045	0.809–1.350	0.737
IC IVP (mg/mL) ≥ 2.4	1.596	0.2179	53.617	4.932	3.218–7.561	0.000
NIC IVP ≥ 0.40	0.259	0.1647	2.462	1.295	0.938–1.789	0.117
λ_{HU} IVP ≥ 1.00	0.493	0.1798	7.511	1.637	1.151–2.328	0.006
Multivariate analysis						
Level						
VIa	0.708	0.2971	5.683	2.030	1.134–3.634	0.017
VIb	1.042	0.2931	12.647	2.836	1.597–5.038	0.000
Diameter (cm) ≥ 0.32	0.704	0.2844	6.135	2.023	1.158–3.532	0.013
IC IAP (mg/mL) ≥ 2.1	1.492	0.2343	40.521	4.444	2.808–7.035	0.000
IC IVP (mg/mL) ≥ 2.4	1.684	0.2274	54.815	5.387	3.449–8.413	0.000

^{*}, set to zero because this parameter is redundant. DECT, dual-energy computed tomography; LNM, lymph node metastasis; GEE, generalized estimating equation; S.E., standard error; OR, odds ratio; CI, confidence intervals; IC, iodine concentration; IAP, in the arterial phase; NIC, normalized iodine concentration; IVP, in the venous phase; λ_{HU} , the slope of the energy spectrum curve.

in the arterial phase, and NIC in the venous phase, had significantly higher accuracy for preoperative diagnosis of metastatic cervical LNs <0.5 cm in patients with PTC. An IC in the arterial phase ≥ 2.1 mg/mL was an optimum single parameter. Metastasis could be considered for LNs meeting the following parameters: located in level VIa or VIb, diameter ≥ 0.32 cm, IC in the arterial phase ≥ 2.1 mg/mL, and IC in the venous phase ≥ 2.4 mg/mL.

To date, the majority of studies on the use of DECT in patients with PTC have focused on metastatic LNs >0.5 cm (18,33). A study by Liu *et al.* (33) showed the best single parameter for the detection of metastatic LNs was λ_{HU} in the venous phase, and Zhao *et al.* (18) showed that the

optimal IC diagnostic threshold was 2.56 mg/mL in the arterial phase. These findings differ from our results, which we believe to be due to the following reasons. DECT can obtain characteristic energy spectrum curves of different substances, as well as single energy images within a certain energy range and CT values at any single energy point. Therefore, λ_{HU} can reflect the attenuation characteristics of lesions under different energy conditions, and λ_{HU} can be used for tissue composition analysis. The iodine map can directly reflect the difference in IC in lesions, especially for LNs <0.5 cm.

In our study, IC, NIC, and λ_{HU} of metastatic LNs were higher than that of non-metastatic LNs in both the arterial

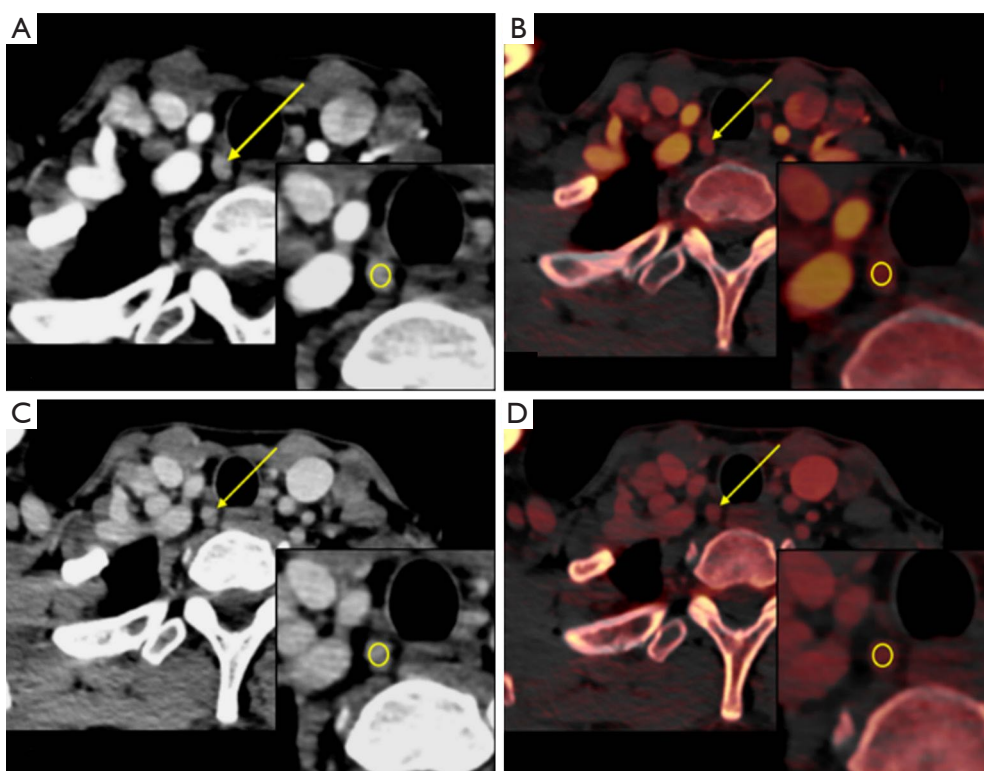


Figure 5 Typical dual-energy CT images and iodine maps of metastatic lymph node with a diameter of 0.47 cm in a 51-year-old woman with PTC. (A) Contrast-enhanced monochromatic image in the arterial phase of a metastatic lymph node (area, 12 mm², CT value, 88.9±12.1 HU). (B) Iodine map in the arterial phase of a metastatic lymph node (area, 12 mm²; iodine concentration, 5.7 mg/mL). (C) Contrast-enhanced monochromatic image in the venous phase of a metastatic lymph node (area, 12 mm², CT value, 78.6±15.1 HU). (D) Iodine map in the venous phase of a metastatic lymph node (area, 12 mm²; iodine concentration, 3.5 mg/mL). CT, computed tomography; PTC, papillary thyroid carcinoma.

and the venous phases, which was consistent with the findings of previous studies (18,33). The main reason for this observation was that non-metastatic LNs had a low blood supply, while metastatic LNs had a high blood supply on account of the specific iodine absorption characteristics of the thyroid, even in small LNs.

This study showed that, among all the quantitative parameters, IC in the arterial phase had the highest sensitivity for differentiating metastatic from non-metastatic LNs. The GEE analysis showed that IC in the venous phase ≥ 2.4 mg/mL was another independent factor affecting LNM. IC has been considered as a direct response to blood flow, and is affected by the number of blood vessels (36). In PTC, normal follicular cells, responsible for thyroid iodine uptake, which exist in benign conditions such as follicular adenoma or nodular hyperplasia, are replaced by cancer cells or fibrotic tissues (37). Therefore, the differences in

iodine uptake might lead to significantly different IC values among metastatic and non-metastatic LNs. The specific iodine absorption characteristics of thyroid tissue and the changes in tumor-related vascular patterns in LNs were also found to be correlated with IC (38). However, some scholars (33,39) have reported NIC to be a relatively stable parameter that could reduce differences among patients to a certain extent, and as being superior to IC in diagnostic efficiency. As IC is a direct measurement, we think it is easier to obtain and less likely to be disturbed by extraneous factors, which was consistent with the results of Zhao *et al.* (18). Moreover, we found that the use of quantitative parameters, especially the combination of diameter, IC in the arterial phase, and NIC in the venous phase, showed a higher AUC compared to the single parameters.

The most common type of metastasis in patients with PTC is lymphatic metastasis (40,41). According to

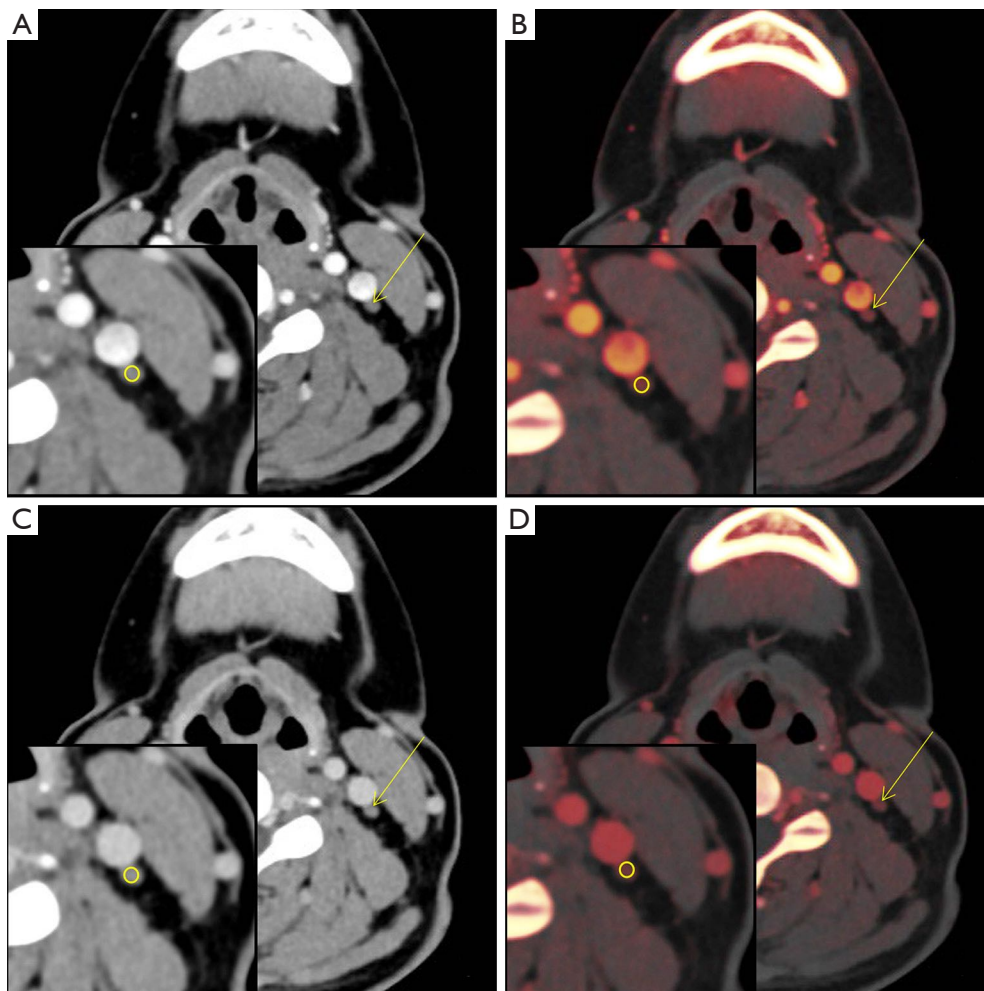


Figure 6 Typical dual-energy CT images and iodine maps of non-metastatic lymph node with a diameter of 0.31 cm in a 37-year-old woman with PTC. (A) Contrast-enhanced monochromatic image in the arterial phase of a metastatic lymph node (area, 15 mm², CT value, 40.2±7.2 HU). (B) Iodine map in the arterial phase of a metastatic lymph node (area, 15 mm²; iodine concentration, 0.8 mg/mL). (C) Contrast-enhanced monochromatic image in the venous phase of a metastatic lymph node (area, 15 mm², CT value, 61.4±6.5 HU). (D) Iodine map in the venous phase of a metastatic lymph node (area, 15 mm²; iodine concentration, 1.3 mg/mL). CT, computed tomography; PTC, papillary thyroid carcinoma.

ATA guidelines (42), the first metastatic region was the central region (VI), which was more common than the cervical region of the ipsilateral neck and the paratracheal metastasis. According to the study of Gregoire *et al.* (35), the majority of the metastatic LNs were around the internal jugular vein, and lymphatic vessels could be transferred to the posterior trigone or mediastinal LNs, but rarely to the submandibular region (Ib) (11,35). In summary, LNs in level VI were more likely to be involved.

The GEE analysis showed that a diameter ≥ 0.32 cm could be regarded as another independent influencing factor for LNM in patients with PTC. We found that for LNs

< 0.5 cm, the greater the diameter, the greater the possibility of metastasis.

Our study has five limitations. First, we employed a retrospective study design, and even though strict inclusion and exclusion criteria were adopted, there was still potential participant selection bias. Second, our study lacked a comparison of morphological features of LNs, besides diameter. However, the purpose of this study was not to evaluate the morphological diagnosis of LNs but to evaluate whether the specific parameters of DECT could identify differences in IC between the two groups. Third, considering the vascular spatial heterogeneity in PTC, a

possible deviation was that a manual ROI may not represent total tumor vascularity. However, the method of manual ROI placement in the solid part of the LN including the entire LN in this study has been verified as a reliable and efficient measurement, and has been widely used in previous studies (33). Fourth, a preoperative US diagnosis of suspected LNs was not performed. Finally, in our study, the correlation of quantitative parameters with the morphology of LNs was not investigated, as this required one-to-one correspondence between pathological morphology and DECT measurements; however, this will be carried out in subsequent studies.

Conclusions

An IC in the arterial phase ≥ 2.1 mg/mL in cervical LNs with a short diameter < 0.5 cm suggested the possibility of metastasis in preoperative DECT examination of patients with PTC. DECT had a higher ability to identify metastasis when the following combination of parameters was taken into consideration: level VIa or VIb, diameter ≥ 0.32 cm, IC in the arterial phase ≥ 2.1 mg/mL, and IC in the venous phase ≥ 2.4 mg/mL.

Acknowledgments

The authors thank: Jianhua Gu, MD, of the Department of General Surgery, Tianjin First Central Hospital for patient recruitment and guidance of clinical work; Wen Shen, MD, of the Department of Radiology, Tianjin First Central Hospital for image acquisition; and Xi Zhao, Senior engineer at Siemens, for their support of dual-energy computed tomography image post-processing.

Funding: This study was supported by the National Natural Science Foundation of China (NSFC, 81871342 to Shuang Xia, 81971585 to Guolin Ma), and the National Key Research and Development Project (2019YFC0120903 to Shuang Xia, 2020YFC2003903 to Guolin Ma).

Footnote

Conflicts of Interest: All authors have completed the ICMJE uniform disclosure form (available at <http://dx.doi.org/10.21037/qims-20-846>). The authors have no conflicts of interest to declare.

Ethical Statement: This retrospective study was approved by the ethics committee of the Tianjin First Central Hospital

(2018N131KY), and the requirement for written informed consent was waived due to its retrospective nature.

Open Access Statement: This is an Open Access article distributed in accordance with the Creative Commons Attribution-NonCommercial-NoDerivs 4.0 International License (CC BY-NC-ND 4.0), which permits the non-commercial replication and distribution of the article with the strict proviso that no changes or edits are made and the original work is properly cited (including links to both the formal publication through the relevant DOI and the license). See: <https://creativecommons.org/licenses/by-nc-nd/4.0/>.

References

1. Carling T, Carty SE, Ciarleglio MM, Cooper DS, Doherty GM, Kim LT, Kloos RT, Mazzaferri EL Sr, Peduzzi PN, Roman SA, Sippel RS, Sosa JA, Stack BC Jr, Steward DL, Tufano RP, Tuttle RM, Udelsman R. American Thyroid Association design and feasibility of a prospective randomized controlled trial of prophylactic central lymph node dissection for papillary thyroid carcinoma. *Thyroid* 2012;22:237-44.
2. Lesnik D, Cunnane ME, Zurakowski D, Acar GO, Ecevit C, Mace A, Kamani D, Randolph GW. Papillary thyroid carcinoma nodal surgery directed by a preoperative radiographic map utilizing CT scan and ultrasound in all primary and reoperative patients. *Head Neck* 2014;36:191-202.
3. Vogl TJ, Schulz B, Bauer RW, Stover T, Sader R, Tawfik AM. Dual-energy CT applications in head and neck imaging. *AJR Am J Roentgenol* 2012;199:S34-9.
4. Mansour J, Sagiv D, Alon E, Talmi Y. Prognostic value of lymph node ratio in metastatic papillary thyroid carcinoma. *J Laryngol Otol* 2018;132:8-13.
5. Lin JD, Hsueh C, Chao TC. Early recurrence of papillary and follicular thyroid carcinoma predicts a worse outcome. *Thyroid* 2009;19:1053-9.
6. Park JH, Yoon JH. Lobectomy in patients with differentiated thyroid cancer: indications and follow-up. *Endocr Relat Cancer* 2019;26: R381-93.
7. Randolph GW, Duh QY, Heller KS, LiVolsi VA, Mandel SJ, Steward DL, Tufano RP, Tuttle RM. The prognostic significance of nodal metastases from papillary thyroid carcinoma can be stratified based on the size and number of metastatic lymph nodes, as well as the presence of extranodal extension. *Thyroid* 2012;22:1144-52.
8. Smith VA, Sessions RB, Lentsch EJ. Cervical lymph node

- metastasis and papillary thyroid carcinoma: does the compartment involved affect survival? Experience from the SEER database. *J Surg Oncol* 2012;106:357-62.
9. Yeh MW, Bauer AJ, Bernet VA, Ferris RL, Loevner LA, Mandel SJ, Orloff LA, Randolph GW, Steward DL. American Thyroid Association statement on preoperative imaging for thyroid cancer surgery. *Thyroid* 2015;25:3-14.
 10. Xu SY, Yao JJ, Zhou W, Chen L, Zhan WW. Clinical characteristics and ultrasonographic features for predicting central lymph node metastasis in clinically node-negative papillary thyroid carcinoma without capsule invasion. *Head Neck* 2019;41:3984-91.
 11. Lee DW, Ji YB, Sung ES, Park JS, Lee YJ, Park DW, Tae K. Roles of ultrasonography and computed tomography in the surgical management of cervical lymph node metastases in papillary thyroid carcinoma. *Eur J Surg Oncol* 2013;39:191-6.
 12. Hwang HS, Orloff LA. Efficacy of preoperative neck ultrasound in the detection of cervical lymph node metastasis from thyroid cancer. *Laryngoscope* 2011;121:487-91.
 13. Khokhar MT, Day KM, Sangal RB, Ahmedli NN, Pisharodi LR, Beland MD, Monchik JM. Preoperative High-Resolution Ultrasound for the Assessment of Malignant Central Compartment Lymph Nodes in Papillary Thyroid Cancer. *Thyroid* 2015;25:1351-4.
 14. Han Z, Lei Z, Li M, Luo D, Ding J. Differential diagnosis value of the ultrasound gray scale ratio for papillary thyroid microcarcinomas and micronodular goiters. *Quant Imaging Med Surg* 2018;8:507-13.
 15. Cheng SCH, Ahuja AT, Ying M. Quantification of intranodal vascularity by computer pixel-counting method enhances the accuracy of ultrasound in distinguishing metastatic and tuberculous cervical lymph nodes. *Quant Imaging Med Surg* 2019;9:1773-80.
 16. Tam AA, Kaya C, Ucler R, Dirikoc A, Ersoy R, Cakir B. Correlation of normal thyroid ultrasonography with thyroid tests. *Quant Imaging Med Surg* 2015;5:569-74.
 17. Liu C, Chen S, Yang Y, Shao D, Peng W, Wang Y, Chen Y, Wang Y. The value of the computer-aided diagnosis system for thyroid lesions based on computed tomography images. *Quant Imaging Med Surg* 2019;9:642-53.
 18. Zhao Y, Li X, Li L, Wang X, Lin M, Zhao X, Luo D, Li J. Preliminary study on the diagnostic value of single-source dual-energy CT in diagnosing cervical lymph node metastasis of thyroid carcinoma. *J Thorac Dis* 2017;9:4758-66.
 19. Kato H, Kanematsu M, Kato Z, Teramoto T, Mizuta K, Aoki M, Makita H, Kato K. Necrotic cervical nodes: usefulness of diffusion-weighted MR imaging in the differentiation of suppurative lymphadenitis from malignancy. *Eur J Radiol* 2013;82:e28-35.
 20. Zhou L, Wang JZ, Wang JT, Wu YJ, Chen H, Wang WB, Cao F, Cheng GX. Correlation analysis of MR/CT on colorectal cancer lymph node metastasis characteristics and prognosis. *Eur Rev Med Pharmacol Sci* 2017;21:1219-25.
 21. Zhang H, Zhang C, Zheng Z, Ye F, Liu Y, Zou S, Zhou C. Chemical shift effect predicting lymph node status in rectal cancer using high-resolution MR imaging with node-for-node matched histopathological validation. *Eur Radiol* 2017;27:3845-55.
 22. Sun H, Zhou J, Liu K, Shen T, Wang X, Wang X. Pancreatic neuroendocrine tumors: MR imaging features preoperatively predict lymph node metastasis. *Abdom Radiol (NY)* 2019;44:1000-9.
 23. Xie T, Li Y, He G, Zhang Z, Shi Q, Cheng G. The influence of liver fat deposition on the quantification of the liver-iron fraction using fast-kilovolt-peak switching dual-energy CT imaging and material decomposition technique: an in vitro experimental study. *Quant Imaging Med Surg* 2019;9:654-61.
 24. Grillet F, Busse-Cote A, Calame P, Behr J, Delabrousse E, Aubry S. COVID-19 pneumonia: microvascular disease revealed on pulmonary dual-energy computed tomography angiography. *Quant Imaging Med Surg* 2020;10:1852-62.
 25. Weidman EK, Plodkowski AJ, Halpenny DE, Hayes SA, Perez-Johnston R, Zheng J, Moskowitz C, Ginsberg MS. Dual-Energy CT Angiography for Detection of Pulmonary Emboli: Incremental Benefit of Iodine Maps. *Radiology* 2018;289:546-53.
 26. Booz C, Noske J, Martin SS, Albrecht MH, Yel I, Lenga L, Gruber-Rouh T, Eichler K, D'Angelo T, Vogl TJ, Wichmann JL. Virtual Noncalcium Dual-Energy CT: Detection of Lumbar Disk Herniation in Comparison with Standard Gray-scale CT. *Radiology* 2019;290:446-55.
 27. Li J, Fang M, Wang R, Dong D, Tian J, Liang P, Liu J, Gao J. Diagnostic accuracy of dual-energy CT-based nomograms to predict lymph node metastasis in gastric cancer. *Eur Radiol* 2018;28:5241-9.
 28. Zhang X, Zheng C, Yang Z, Cheng Z, Deng H, Chen M, Duan X, Mao J, Shen J. Axillary Sentinel Lymph Nodes in Breast Cancer: Quantitative Evaluation at Dual-Energy CT. *Radiology* 2018;289:337-46.
 29. Ji GW, Zhang YD, Zhang H, Zhu FP, Wang K, Xia YX, Zhang YD, Jiang WJ, Li XC, Wang XH. Biliary Tract Cancer at CT: A Radiomics-based Model to

- Predict Lymph Node Metastasis and Survival Outcomes. *Radiology* 2019;290:90-8.
30. Zeng YR, Yang QH, Liu QY, Min J, Li HG, Liu ZF, Li JX. Dual energy computed tomography for detection of metastatic lymph nodes in patients with hepatocellular carcinoma. *World J Gastroenterol* 2019;25:1986-96.
 31. Haddad RI, Nasr C, Bischoff L, Busaidy NL, Byrd D, Callender G, Dickson P, Duh QY, Ehya H, Goldner W, Haymart M, Hoh C, Hunt JP, Iagaru A, Kandeel F, Kopp P, Lamonica DM, McIver B, Raeburn CD, Ridge JA, Ringel MD, Scheri RP, Shah JP, Sippel R, Smallridge RC, Sturgeon C, Wang TN, Wirth LJ, Wong RJ, Johnson-Chilla A, Hoffmann KG, Gurski LA. NCCN Guidelines Insights: Thyroid Carcinoma, Version 2.2018. *J Natl Compr Canc Netw* 2018;16:1429-40.
 32. Rizzo S, Radice D, Femia M, De Marco P, Origgi D, Preda L, Barberis M, Vigorito R, Mauri G, Mauro A, Bellomi M. Metastatic and non-metastatic lymph nodes: quantification and different distribution of iodine uptake assessed by dual-energy CT. *Eur Radiol* 2018;28:760-9.
 33. Liu X, Ouyang D, Li H, Zhang R, Lv Y, Yang A, Xie C. Papillary thyroid cancer: dual-energy spectral CT quantitative parameters for preoperative diagnosis of metastasis to the cervical lymph nodes. *Radiology* 2015;275:167-76.
 34. Park JE, Lee JH, Ryu KH, Park HS, Chung MS, Kim HW, Choi YJ, Baek JH. Improved Diagnostic Accuracy Using Arterial Phase CT for Lateral Cervical Lymph Node Metastasis from Papillary Thyroid Cancer. *AJNR Am J Neuroradiol* 2017;38:782-8.
 35. Gregoire V, Ang K, Budach W, Grau C, Hamoir M, Langendijk JA, Lee A, Le QT, Maingon P, Nutting C, O'Sullivan B, Porceddu SV, Lengele B. Delineation of the neck node levels for head and neck tumors: a 2013 update. DAHANCA, EORTC, HKNPCSG, NCIC CTG, NCRI, RTOG, TROG consensus guidelines. *Radiother Oncol* 2014;110:172-81.
 36. Tawfik AM, Michael Bucher A, Vogl TJ. Dual-Energy Computed Tomography Applications for the Evaluation of Cervical Lymphadenopathy. *Neuroimaging Clin N Am* 2017;27:461-8.
 37. Galrao AL, Camargo RY, Friguglietti CU, Moraes L, Cerutti JM, Serrano-Nascimento C, Suzuki MF, Medeiros-Neto G, Rubio IG. Hypermethylation of a New Distal Sodium/Iodide Symporter (NIS) enhancer (NDE) is associated with reduced NIS expression in thyroid tumors. *J Clin Endocrinol Metab* 2014;99:E944-52.
 38. Vergez S, Sarini J, Percodani J, Serrano E, Caron P. Lymph node management in clinically node-negative patients with papillary thyroid carcinoma. *Eur J Surg Oncol* 2010;36:777-82.
 39. Tawfik AM, Razek AA, Kerl JM, Nour-Eldin NE, Bauer R, Vogl TJ. Comparison of dual-energy CT-derived iodine content and iodine overlay of normal, inflammatory and metastatic squamous cell carcinoma cervical lymph nodes. *Eur Radiol* 2014;24:574-80.
 40. Mamelle E, Borget I, Leboulleux S, Mirghani H, Suarez C, Pellitteri PK, Shaha AR, Hamoir M, Robbins KT, Khaffi A, Rodrigo JP, Silver CE, Rinaldo A, Ferlito A, Hartl DM. Impact of prophylactic central neck dissection on oncologic outcomes of papillary thyroid carcinoma: a review. *Eur Arch Otorhinolaryngol* 2015;272:1577-86.
 41. Li L, Wang Y, Luo DH, Zhao YF, Lin M, Guo W, Hu L, Zhou CW, Zhao XM. Diagnostic value of single-source dual-energy spectral computed tomography for papillary thyroid microcarcinomas. *J Xray Sci Technol* 2017;25:793-802.
 42. Haugen BR, Alexander EK, Bible KC, Doherty GM, Mandel SJ, Nikiforov YE, Pacini F, Randolph GW, Sawka AM, Schlumberger M, Schuff KG, Sherman SI, Sosa JA, Steward DL, Tuttle RM, Wartofsky L. 2015 American Thyroid Association Management Guidelines for Adult Patients with Thyroid Nodules and Differentiated Thyroid Cancer: The American Thyroid Association Guidelines Task Force on Thyroid Nodules and Differentiated Thyroid Cancer. *Thyroid* 2016;26:1-133.

Cite this article as: Zou Y, Zheng M, Qi Z, Guo Y, Ji X, Huang L, Gong Y, Lu X, Ma G, Xia S. Dual-energy computed tomography could reliably differentiate metastatic from non-metastatic lymph nodes of less than 0.5 cm in patients with papillary thyroid carcinoma. *Quant Imaging Med Surg* 2021;11(4):1354-1367. doi: 10.21037/qims-20-846

The reason why DECT was applied in patients with PTC

The success of surgery for thyroid cancer hinges on thorough and accurate preoperative imaging, which enables complete clearance of the primary tumor and affected lymph node compartments. Although US is a standard modality for the assessment of cervical LNM in patients with thyroid cancer, there has been an increasing trend in the number of articles describing the use of contrast-enhanced CT. We searched multiple databases, including PubMed, Web of Science, and Medline, using “CT” and “thyroid cancer” as keywords, and retrieved 16 relevant studies from the past 5 years (18,34,35,43-45). The value of CT examination in patients with thyroid cancer has been evidenced by these studies.

The literature cited by many articles on the application of DECT in the diagnosis of PTC and cervical LNM was

published in *Radiology* in 2015 (34); this study has been cited many times in recent years. This reference evaluated the use of DECT quantitative parameters compared with the use of conventional CT imaging features for the preoperative diagnosis of metastasis of the cervical lymph nodes in patients with PTC. The results showed that DECT quantitative parameters had higher accuracy than the qualitative assessment of conventional CT imaging features for preoperative diagnosis of metastatic cervical lymph nodes in patients with PTC.

Besides, a systematic review and meta-analysis published in *European Radiology* in 2019 studied the diagnostic performance of contrast-enhanced CT, and the results showed that CT demonstrated an acceptable diagnostic performance in the pre- and postoperative diagnosis of metastatic cervical LNs in patients with thyroid cancer (45).

We have listed only two classic references above. The other 14 references also support the value of CT in the

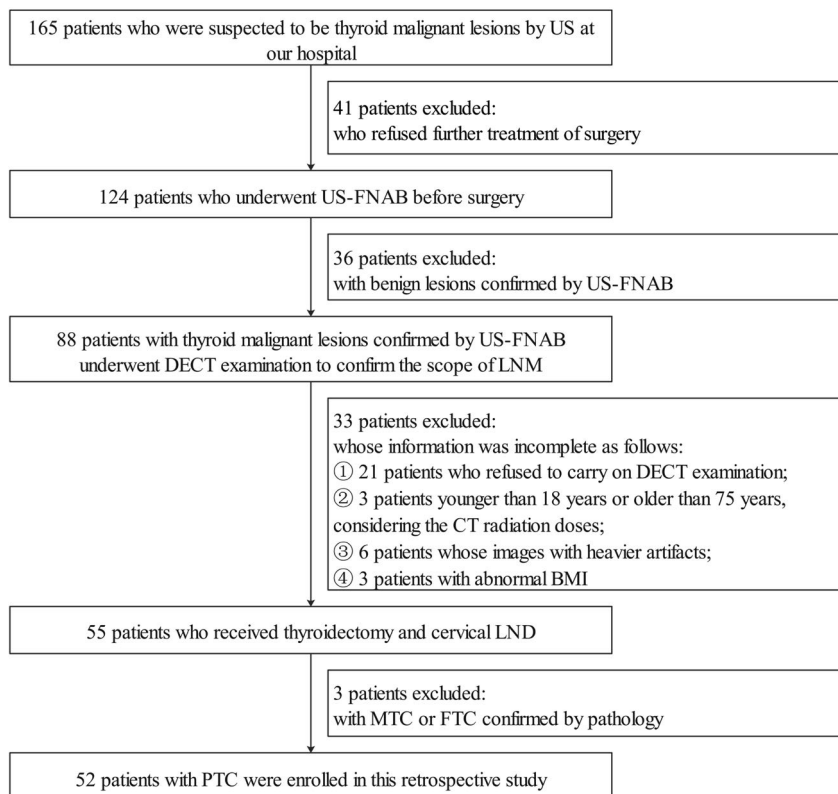


Figure S1 Flowchart showing criteria of inclusion and exclusion for patients with PTC. US, ultrasound; US-FNAB, ultrasound-guided fine needle aspiration biopsy; DECT, dual-energy computed tomography; LNM, lymph node metastasis; BMI, body mass index; LND, lymph node dissection; MTC, medullary thyroid carcinoma; FTC, follicular thyroid carcinoma; PTC, papillary thyroid carcinoma.

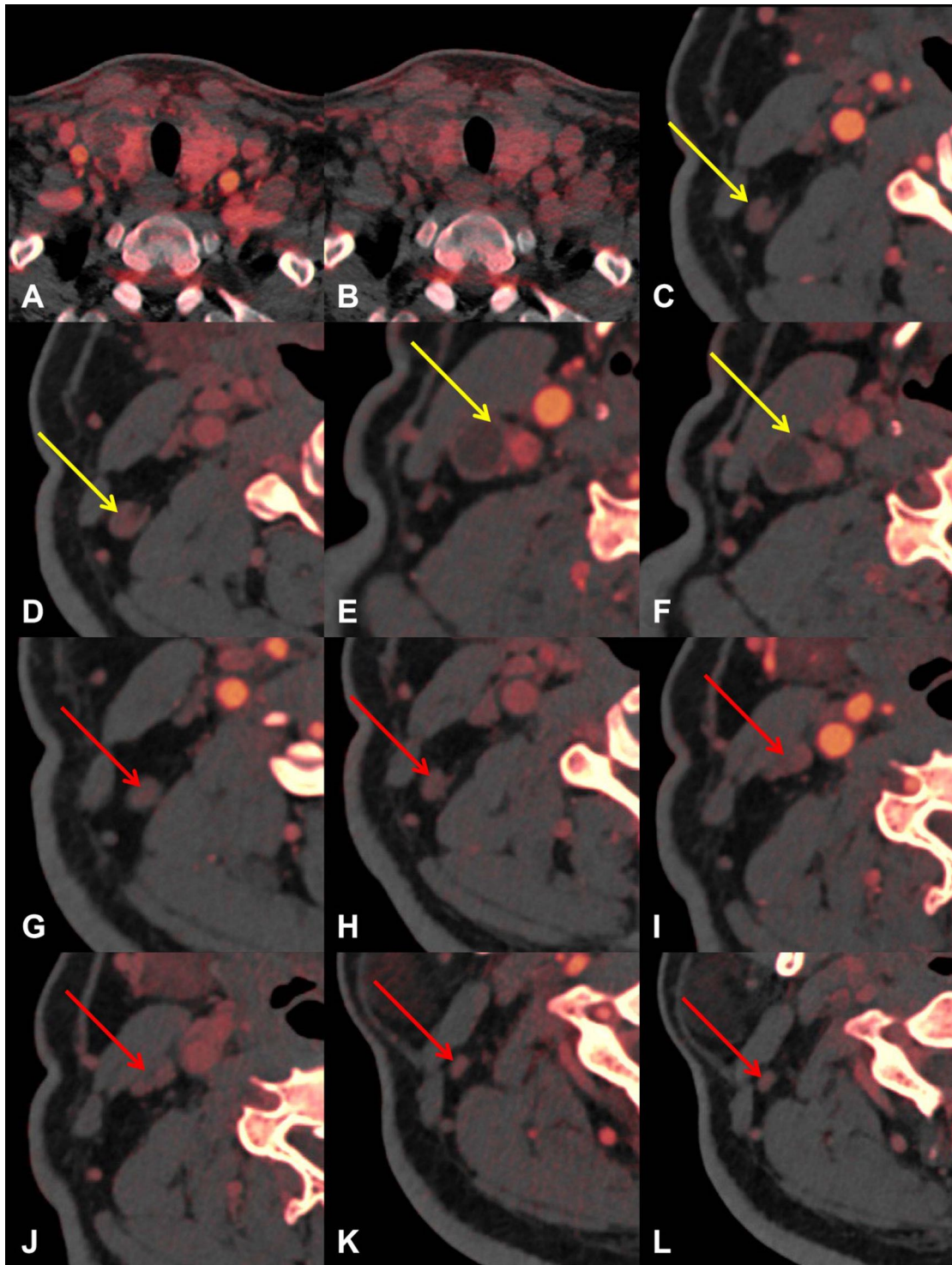


Figure S2 An example in which one level is full of metastatic LNs. Male, 30 years old, total thyroidectomy accompanied by bilateral neck LNs dissection. Postoperative pathological results showed that diffuse PTC and LNs metastasis in right level II (5/5). (A,B) Arterial and venous iodine maps of primary lesions; (C-F) two LNs with a short diameter ≥ 0.5 cm (yellow arrow); (G-L) another three LNs with short diameter < 0.5 cm (red arrow). We only included three LNs < 0.5 cm, and two LNs ≥ 0.5 cm were excluded. LNs, lymph nodes; PTC, papillary thyroid carcinoma.

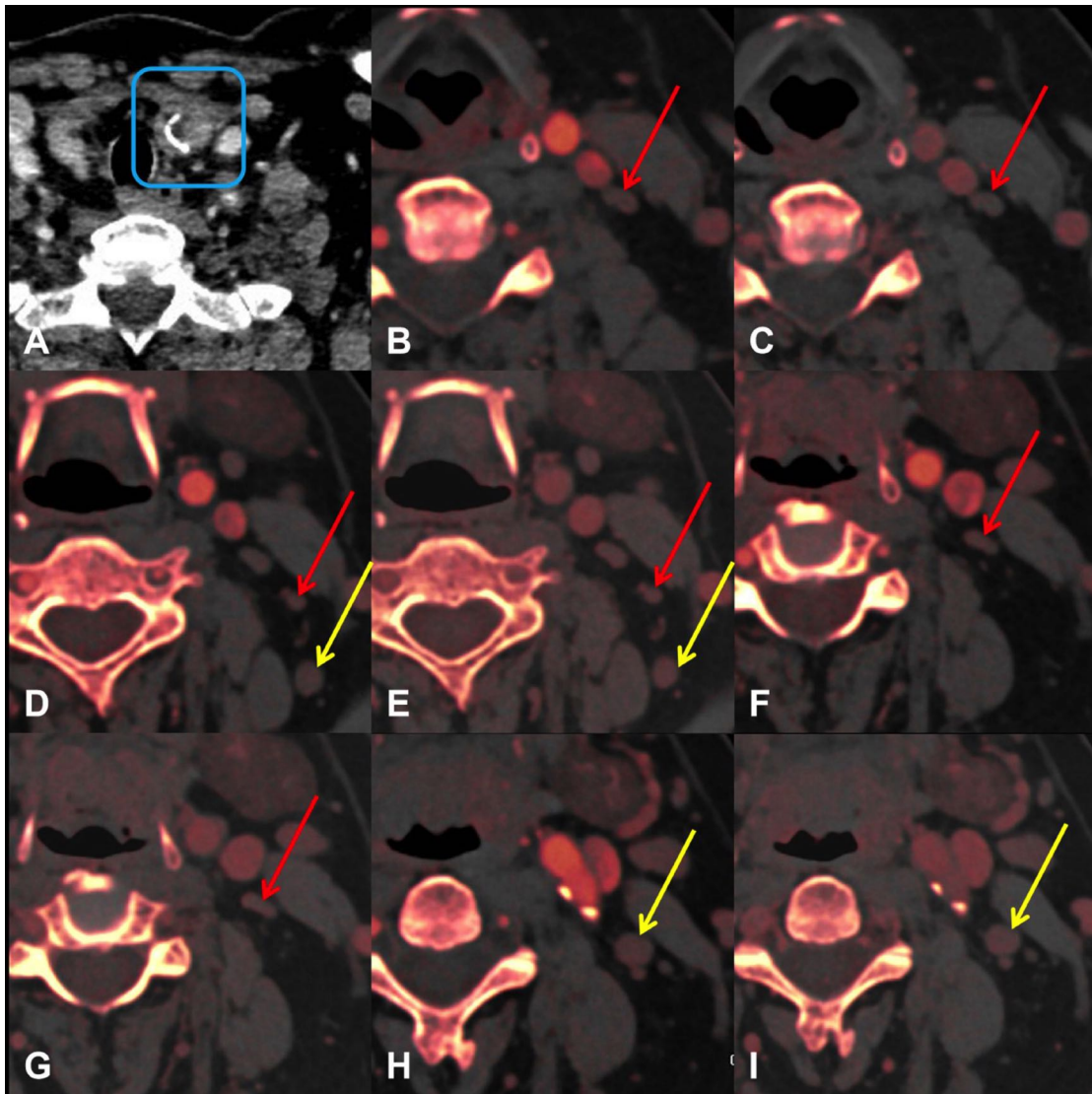


Figure S3 Another example in which one level is full of non-metastatic LNs. Female, 59 years old, left thyroid lobectomy accompanied with left cervical LNs dissection. Postoperative pathological results showed that the left thyroid lobe was considered to be papillary thyroid microcarcinoma with calcification. There were no metastatic LNs in the left level II (0/5). (A) Arterial phase image of the primary tumor (blue square); (B-H) three LNs with short diameter $<0.5\text{ cm}$ (red arrow) in the arterial and the venous phases. (E-I) Another two LNs with a short diameter $\geq 0.5\text{ cm}$ (yellow arrow) in the arterial and the venous phases. We only included three LNs $<0.5\text{ cm}$, and two LNs $\geq 0.5\text{ cm}$ were excluded. LNs, lymph nodes.

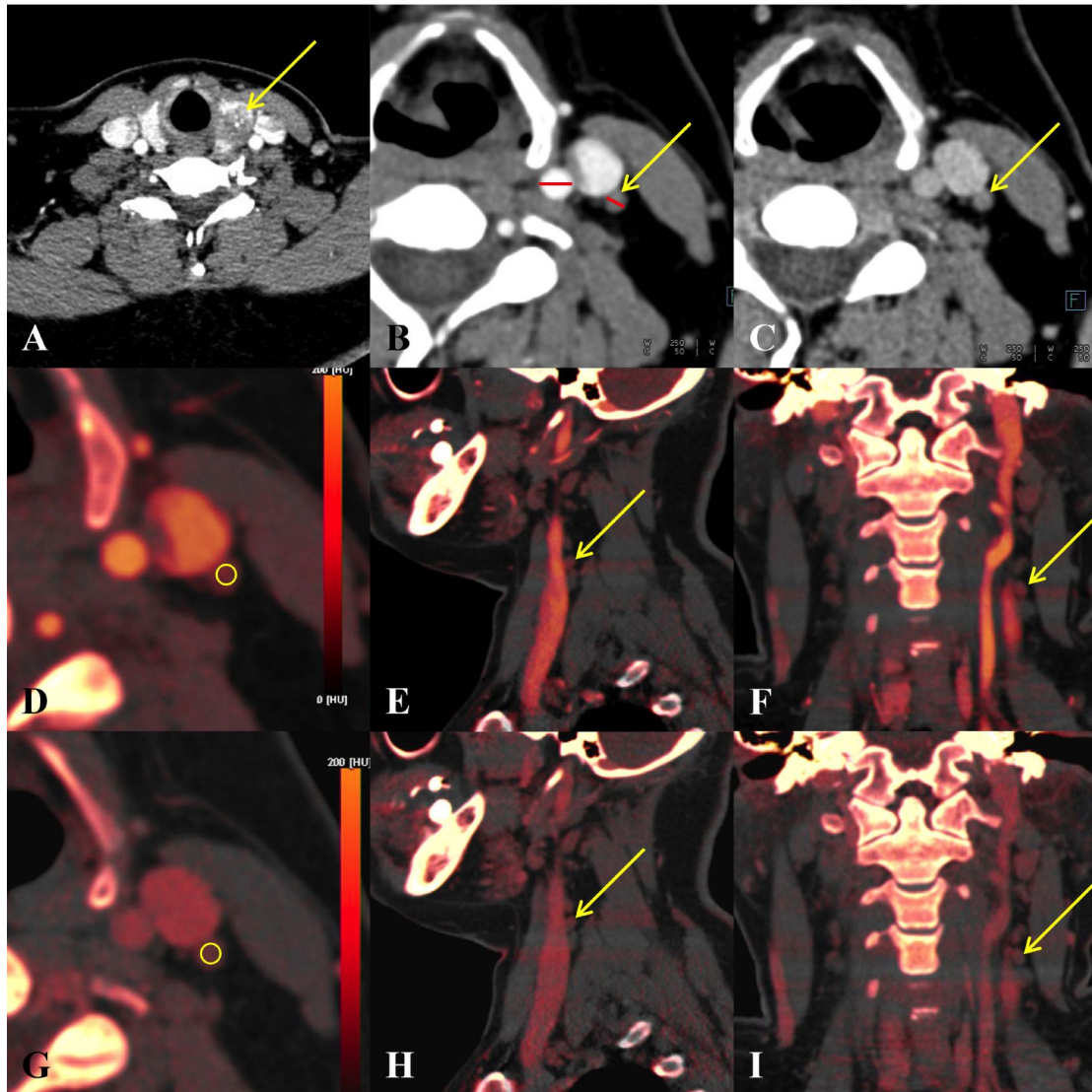


Figure S4 Illustration of specific methods for IC measurement. Female, 36 years old, total thyroidectomy and cervical LN dissection were performed. Pathology confirmed PTC of left lobe with a diameter 1.7 cm (A) all three lymph nodes in the left level IV were metastatic. We measured one of the LNs (diameter of 0.35 cm) as an example. First, by observing the original images of the selected LN in the arterial and the venous phases (B,C), it was determined that the lesion contained enough solid parts to be measured excluding cystic degeneration, necrosis, or calcification. Then, we found the corresponding LN on the iodine map. Under the premise of ensuring sufficient clear resolution, the LN was enlarged in the axial images (D,G), and the ROI was placed on the solid part of the lesion during measurement, excluding cystic degeneration, necrosis, or calcification, and ensuring that it did not include adjacent blood vessels. We comprehensively observed the axial, sagittal (E,H), and coronal (F,I) directions to ensure the accuracy of the measurement. For comparison, the diameter of the common carotid artery on the same plane that was simultaneously measured was 0.7 cm (B). IC, iodine concentration; LN, lymph node; PTC, papillary thyroid carcinoma; LNs, lymph nodes; ROI, region of interest.

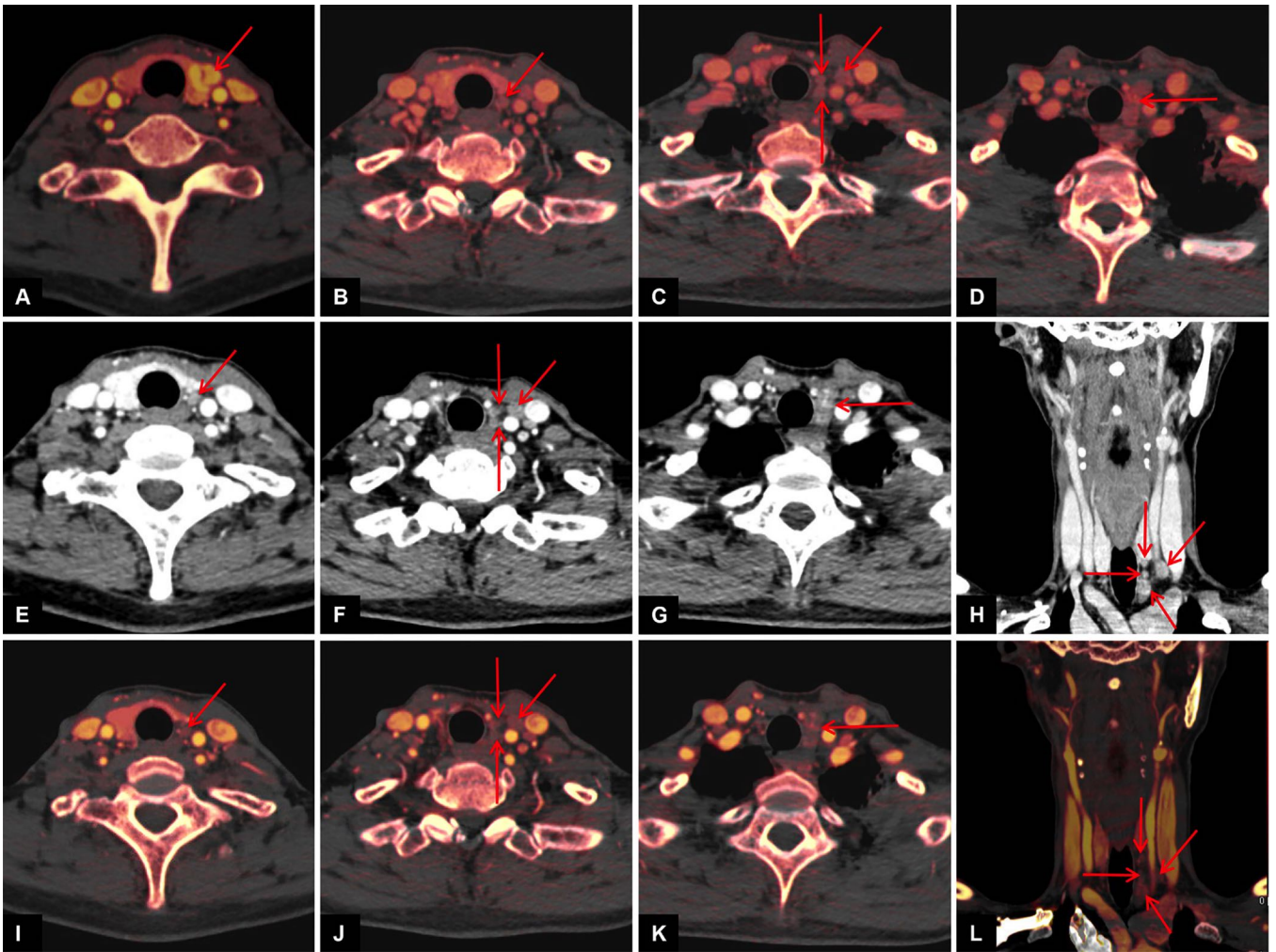


Figure S5 An example of pathological results and DECT both showing that all metastatic lymph nodes are in one level. Female, 52 years old. Left lobe and left level VI dissection were performed. Pathology confirmed PTC of the left lobe with a diameter 1.1 cm (A) and five metastatic LNs were found in the left level VIb. From the DECT images, we also found five metastatic LNs in the left level VIb on the iodine map in the arterial phase (red arrow, B-D) and on contrast-enhanced arterial phase (red arrow, E-H), the ICs of these metastatic LNs were 4.2, 3.1, 3.3, 3.2, and 4.4 mg/mL, respectively. In the venous phase, the ICs of these five metastatic LNs were 4.5, 3.4, 3.1, 3.1, and 3.7 mg/mL, respectively (red arrow, I-L). DECT, dual-energy computed tomography; PTC, papillary thyroid carcinoma; LNs, lymph nodes; ICs, iodine concentrations.

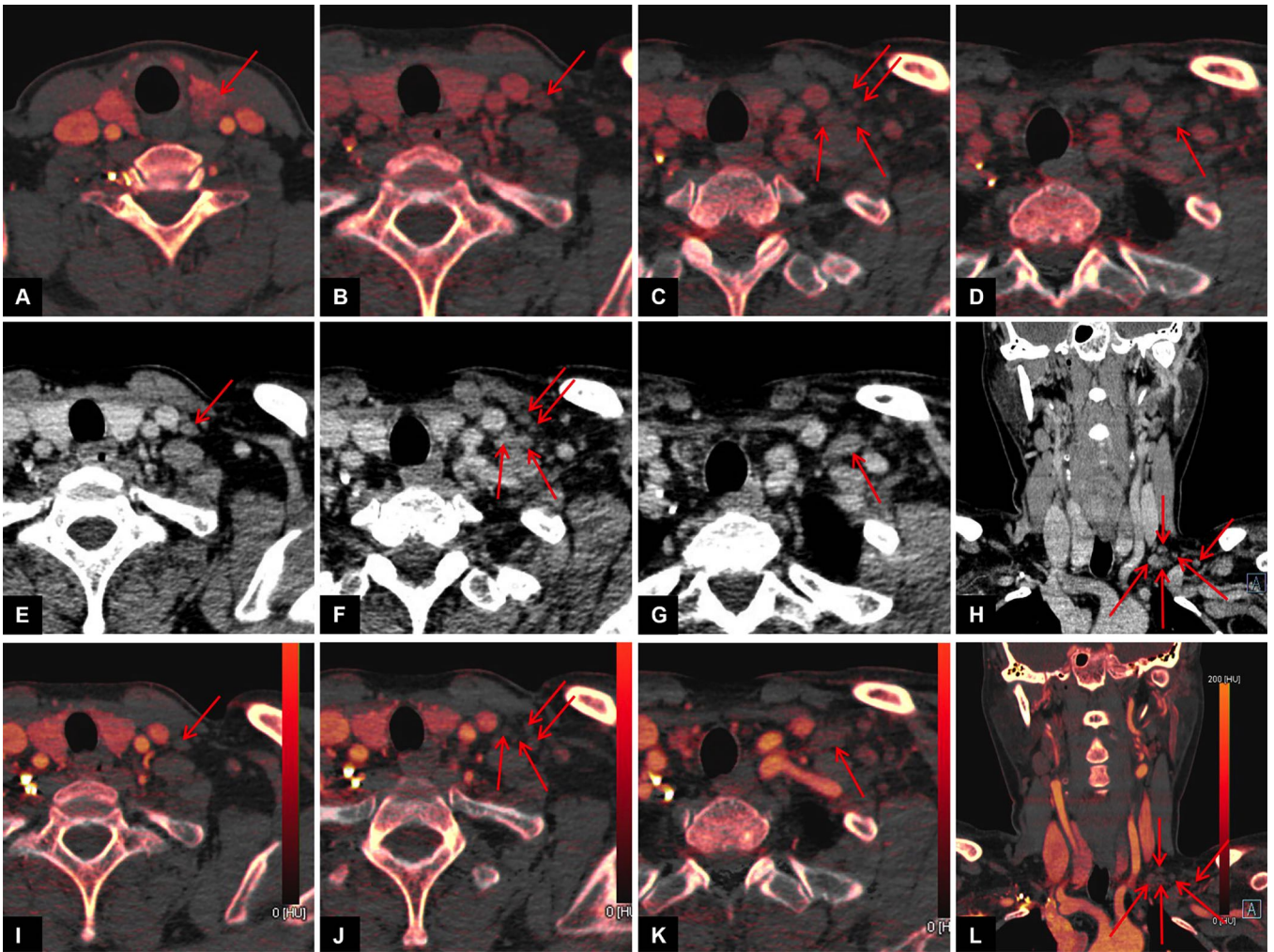


Figure S6 An example of pathological results and DECT both showing that all benign LNs were in one level. Female, 48 years old, left lobe of the thyroid and left level VI dissection was performed. Pathology confirmed PTC of the left lobe with a diameter 2.0 cm (A) no metastatic LNs in the left level VIb were found among six dissected LNs. From the DECT images, we found six LNs in the left level VIb, and all were considered benign (B-D) iodine map in the arterial phase and on contrast-enhanced arterial phase (E-H). The ICs of these LNs were 2.2, 1.4, 2.1, 1.9, 2.4, and 1.8 mg/mL, respectively. In the venous phase, the ICs of these six metastatic LNs were 2.0, 1.4, 1.8, 1.7, 2.1, and 1.7 mg/mL, respectively (I-L). DECT, dual-energy computed tomography; LNs, lymph nodes; PTC, papillary thyroid carcinoma; ICs, iodine concentrations.

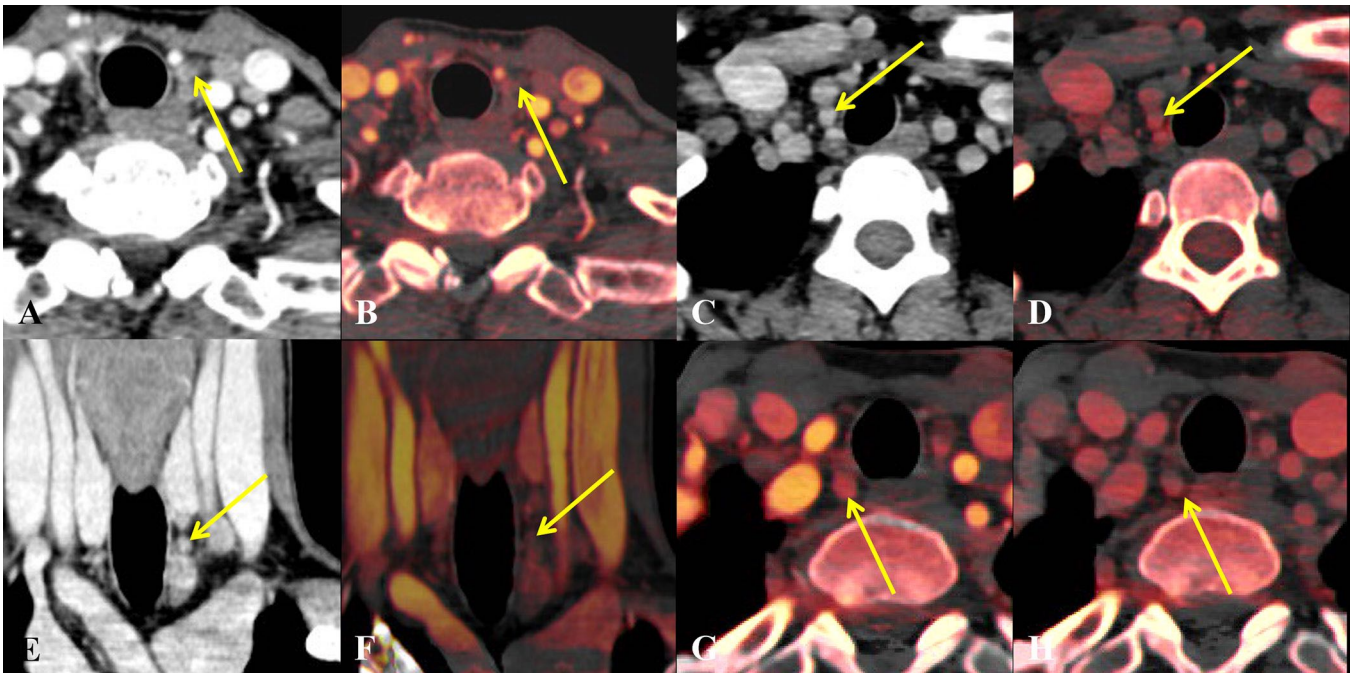


Figure S7 Illustration of the specific criteria for DECT to diagnose metastatic LN. (A,B) A metastatic LN with cystic degeneration and heterogeneous enhancement in the left level VIb. (C,D) A metastatic LN with strong enhancement in the right level VIb. (E,F) A metastatic LN with micro-calcification in the left level VIb. (G,H) A metastatic LN in the right level VIb with IC of 4.7 mg/mL in the arterial phase, and 3.7 mg/mL in the venous phase. DECT, dual-energy computed tomography; IC, iodine concentration; LN, lymph node; IC, iodine concentration.

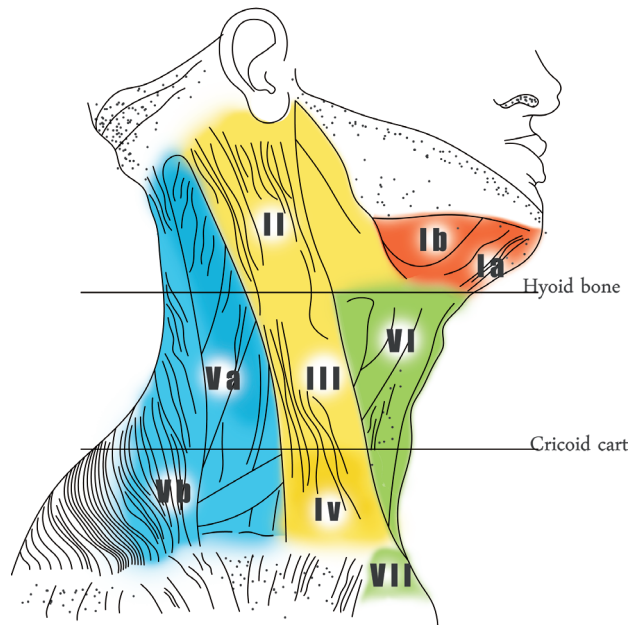


Figure S8 Schematic diagram of cervical LN division. LN, lymph node.

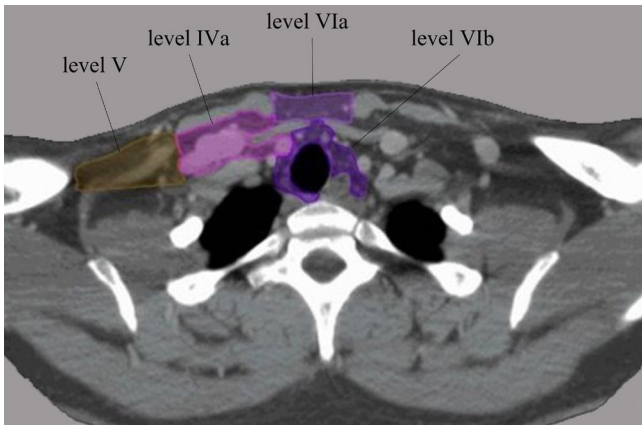


Figure S9 The boundaries of levels VIa and VIb. Level VI contains the anterior compartment nodes including superficially, the anterior jugular nodes (level VIa), and in the deep pre-visceral space, the pre-laryngeal, pre-tracheal, and para-tracheal (recurrent laryngeal nerve) nodes (level VIb). Level VIb receives efferent lymphatics from the anterior floor of the mouth, the tip of the tongue, the lower lip, the thyroid gland, the glottic and subglottic larynx, the hypopharynx, and the cervical esophagus. These nodes are at high risk of metastasis from cancers of the lower lip, the oral cavity, the thyroid gland, the glottic and subglottic larynx, the apex of the piriform sinus, and the cervical esophagus.

Table S1 Demographic, clinical, and pathological characteristics of participants

Characteristic	Statistical data
No. of patients	52
Sex, n (%)	
Male	11 (21.2)
Female	41 (78.8)
Age, years	44.3±11.4
Pathological type, n (%)	
PTC	36 (41.9)
PTMC	50 (58.1)
Multiple, n (%)	
Single	30 (57.7)
Multiple	22 (42.3)
Location, n (%)	
Left lobe	35 (40.7)
Right lobe	42 (48.8)
Isthmus	9 (10.5)
No. of subregions of LNs, n (%)	
Non-metastatic	101 (52.9)
Metastatic	90 (47.1)
No. of LNs, n (%)	
Non-metastatic	220 (61.3)
Metastatic	139 (38.7)

PTC, papillary thyroid carcinoma; PTMC, papillary thyroid microcarcinoma; LNs, lymph nodes.

Table S2 The boundaries of level VIa and VIb

Boundaries	Level VIa	Level VIb
Anterior	Skin or platysma muscle	Posterior aspect of infrahyoid muscle
Posterior	Anterior aspect of the infrahyoid muscle	Anterior aspect of the larynx, thyroid gland, and trachea
Cranial	Caudal edge of the hyoid bone or the submandibular gland	Caudal edge of the thyroid cartilage
Caudal	Cranial edge of the sternal manubrium	Cranial edge of the sternal manubrium
Lateral	Anterior edges of both sternocleidomastoid muscles	Common carotid artery on both sides
Medial	N/A	Lateral aspect of the trachea and esophagus

Table S3 Consistency analysis of the measurement parameters of the two radiologists

Parameters	ICC (95% CI)	P value
Diameter		
Doctor A	0.957 (0.921–0.976)	<0.001
Doctor B	0.958 (0.927–0.976)	<0.001
Doctor A and Doctor B	0.959 (0.919–0.978)	<0.001
IC in the arterial phase		
Doctor A	0.957 (0.925–0.975)	<0.001
Doctor B	0.958 (0.927–0.976)	<0.001
Doctor A and Doctor B	0.945 (0.657–0.981)	<0.001
IC in the venous phase		
Doctor A	0.984 (0.972–0.991)	<0.001
Doctor B	0.984 (0.972–0.991)	<0.001
Doctor A and Doctor B	0.978 (0.430–0.994)	<0.001

IC, iodine concentration; ICC, intraclass correlation coefficient; CI, confidence interval.

Table S5 Multicollinearity assessment in the prediction model based on the independent predictors

Predictors	Collinearity Statistics	
	Tolerance	VIF
Level	0.966	1.035
Diameter	0.981	1.019
ICIAP	0.762	1.313
ICIVP	0.790	1.265

VIF, variance inflation factor; ICIAP, iodine concentration in the arterial phase; ICIVP, iodine concentration in the venous phase.

Table S4 The differences among the AUCs of quantitative parameters

	DBA	95% CI	0.100	Z	P value
IC IAP vs. IC IVP	0.0216	-0.0396 to 0.0828		0.691	0.4895
IC IAP vs. NIC IAP	0.0151	-0.0146 to 0.0448		0.995	0.3198
IC IAP vs. NIC IVP	0.0241	-0.0402 to 0.0885		0.735	0.4622
IC IAP vs. λ_{HU} IAP	0.0974	0.042 to 0.153		3.451	0.0006
IC IAP vs. λ_{HU} IVP	0.165	0.0934 to 0.237		4.52	<0.0001
IC IVP vs. NIC IAP	0.00652	-0.0563 to 0.0694		0.203	0.8388
IC IVP vs. NIC IVP	0.00253	-0.0294 to 0.0344		0.156	0.8763
IC IVP vs. λ_{HU} IAP	0.0758	0.00766 to 0.144		2.18	0.0292
IC IVP vs. λ_{HU} IVP	0.143	0.0854 to 0.201		4.847	<0.0001
NIC IAP vs. NIC IVP	0.00906	-0.0511 to 0.0692		0.295	0.768
NIC IAP vs. λ_{HU} IAP	0.0823	0.0215 to 0.143		2.651	0.008
NIC IAP vs. λ_{HU} IVP	0.15	0.0745 to 0.225		3.899	0.0001
NIC IVP vs. λ_{HU} IAP	0.0733	0.00347 to 0.143		2.057	0.0396
NIC IVP vs. λ_{HU} IVP	0.141	0.0753 to 0.206		4.21	<0.0001
λ_{HU} IAP vs. λ_{HU} IVP	0.0676	0.00629 to 0.129		2.161	0.0307

AUC, area under the curve; CI, confidence interval; DBA, difference between areas; IC, iodine concentration; NIC, normalized iodine concentration; λ_{HU} , the slope of energy spectrum curve; IAP, in the arterial phase; IVP, in the venous phase.

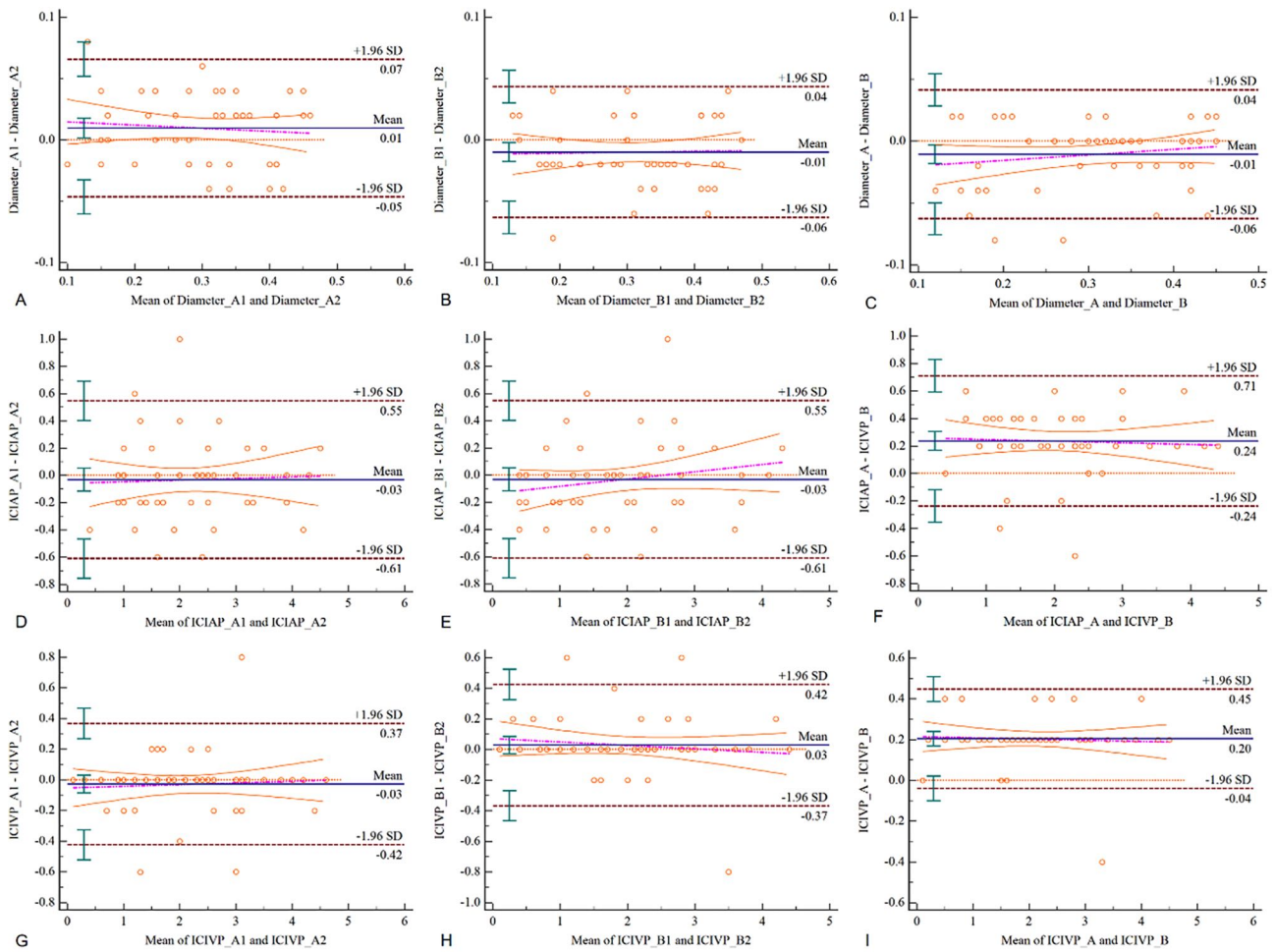


Figure S10 The inter- and intra-observer consistency analyses. The inter-observer consistency analysis result for the ICC of the diameter diagnostic test between doctor A and doctor B was 0.959 ($P < 0.001$), and the intra-observer consistency analysis result for the diameter was 0.957 ($P < 0.001$) and 0.958 ($P < 0.001$) for doctor A and doctor B, respectively (A-C). The inter-observer consistency analysis result for the ICC of the IC in the arterial phase diagnostic test between doctor A and doctor B was 0.945 ($P < 0.001$), and the intra-observer consistency analysis result for the IC in the arterial phase was 0.957 ($P < 0.001$) and 0.958 ($P < 0.001$) for doctor A and doctor B, respectively (D-F). The inter-observer consistency analysis result for the ICC of the IC in the venous phase diagnostic test between doctor A and doctor B was 0.978 ($P < 0.001$), and the intra-observer consistency analysis result for the IC in the venous phase was 0.984 ($P < 0.001$) and 0.984 ($P < 0.001$) for doctor A and doctor B, respectively (G-I). ICC, intraclass correlation coefficient; IC, iodine concentration.

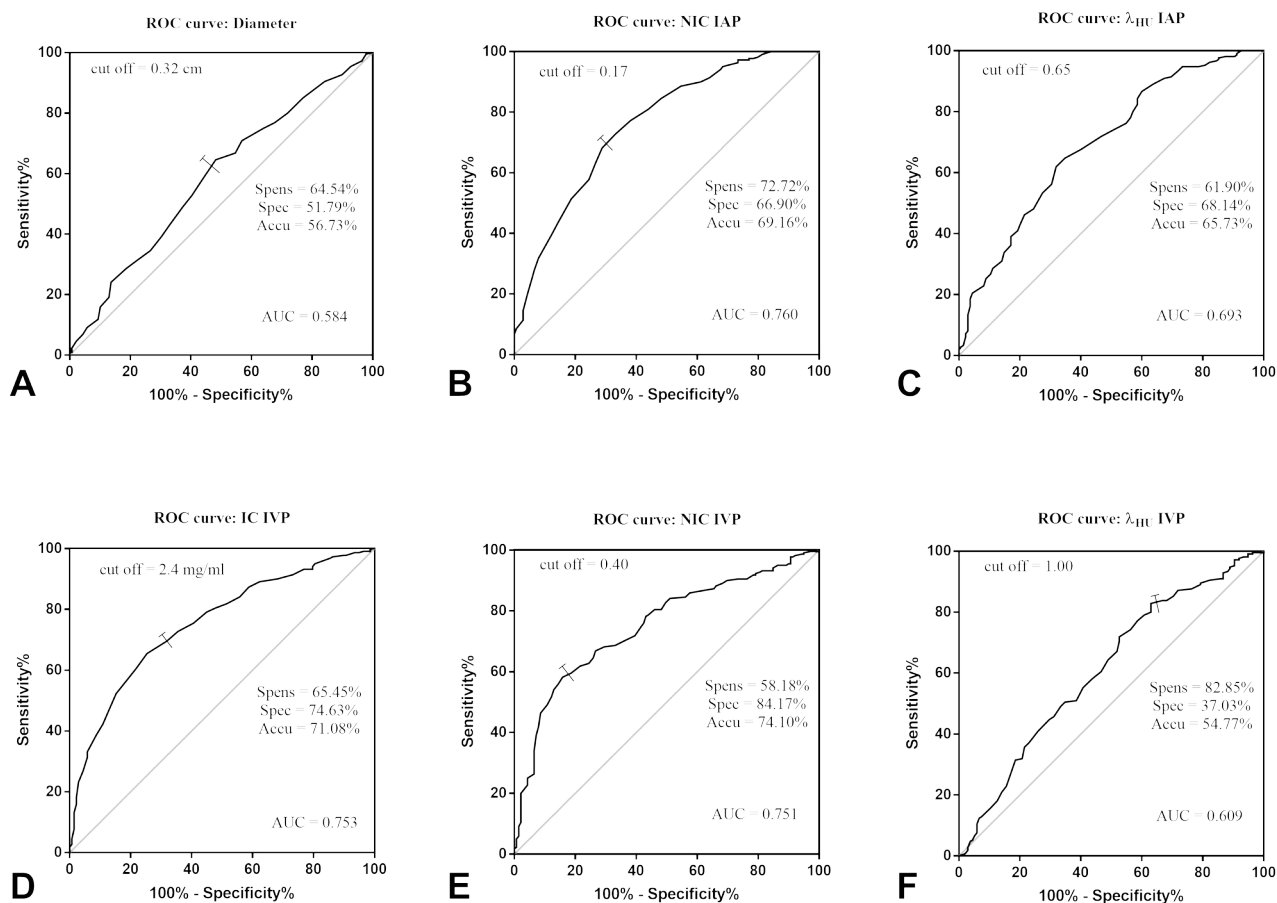


Figure S11 The ROC curves of the quantitative parameters derived from DECT. (A) The AUC, sensitivity, specificity, and accuracy of diameter were 0.584, 64.54%, 51.79%, and 56.73%, respectively, with a cut-off value of 0.32 cm. (B) The AUC, sensitivity, specificity, and accuracy of NIC in the arterial phase were 0.760, 72.72%, 66.90%, and 69.16%, respectively, with a cut-off value of 0.17. (C) The AUC, sensitivity, specificity, and accuracy of λ_{HU} in the arterial phase were 0.693, 61.90%, 68.14%, and 65.73%, respectively, with a cut-off value of 0.65. (D) The AUC, sensitivity, specificity, and accuracy of IC in the venous phase were 0.753, 65.45%, 74.63%, and 71.08%, respectively, with a cut-off value of 2.4 mg/mL. (E) The AUC, sensitivity, specificity, and accuracy of NIC in the venous phase were 0.751, 58.18%, 84.17%, and 74.10%, respectively, with a cut-off value of 0.40. (F) The AUC, sensitivity, specificity, and accuracy of λ_{HU} in the venous phase were 0.609, 82.85%, 37.03%, and 54.77%, respectively, with a cut-off value of 1.00. ROC, receiver operating characteristic; NIC, normalized iodine concentration; IAP, in the arterial phase; λ_{HU} , the slope of energy spectrum curve; IC, iodine concentration; IVP, in the venous phase; DECT, dual-energy computed tomography; AUC, area under the curve

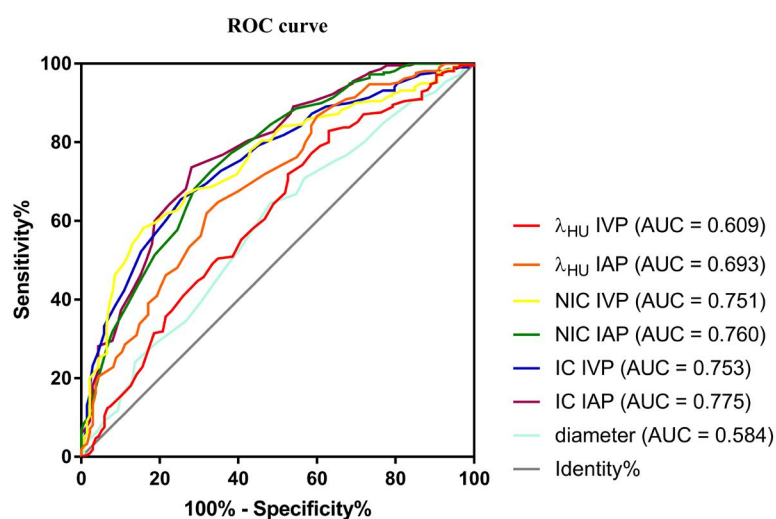


Figure S12 The mixed ROC curves of the quantitative parameters derived from DECT. The AUC was a global measure of the ability of a test to discriminate whether a specific condition was present or not present. An AUC of 0.5 represented a test with no discrimination, while an AUC of 1.0 represented a test with perfect discrimination. The AUCs of diameter, IC IAP, IC IVP, NIC IAP, NIC IVP, λ_{HU} IAP, and λ_{HU} IVP were 0.584, 0.775, 0.753, 0.760, 0.751, 0.693, and 0.609, respectively. Among them, IC IAP had the highest AUC, indicating that it was the most significant for the differentiation of metastatic and non-metastatic LNs. ROC, receiver operating characteristic; DECT, dual-energy computed tomography; AUC, area under the curve; IC, iodine concentration; IAP, in the arterial phase; IVP, in the venous phase; NIC, normalized iodine concentration; λ_{HU} , the slope of energy spectrum curve; LNs, lymph nodes.

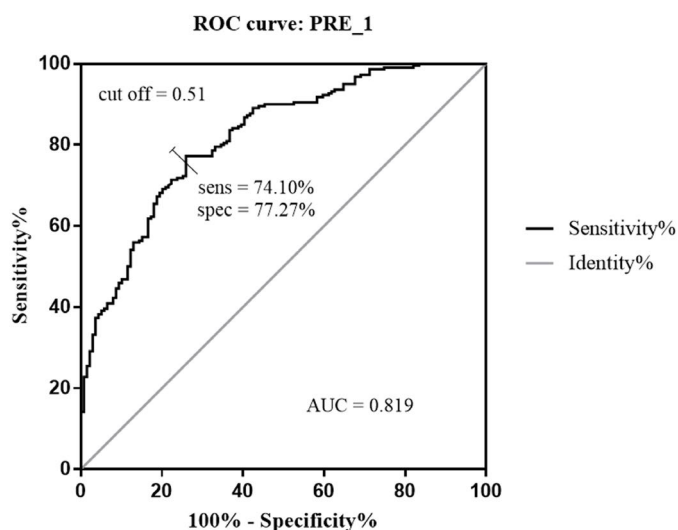


Figure S13 The ROC curve of three combined parameters (diameter, IC in the arterial phase, and NIC in the venous phase) was used to identify metastatic and non-metastatic lymph nodes. When the cut-off value with 0.51, the sensitivity, and specificity were 74.10%, and 77.27%, respectively. The 95% CI: was 0.776–0.858. PRE, prediction probability; ROC, receiver operating characteristic; IC, iodine concentration; NIC, normalized iodine concentration; AUC, area under the curve; CI, confidence interval.

diagnosis of thyroid cancer, we simply did not repeat them here. In addition to the relevant literature, we also consulted the international and domestic guidelines on thyroid cancer and extracted the relevant introductions about CT, which are described in detail below.

The American Thyroid Association (ATA) statement on preoperative imaging for thyroid cancer surgery (9) highlighted that contrast CT may be applied to evaluate lymphadenopathy fully when physical examination and/or US suggest bulky or extensive nodal metastasis is unable to be completely evaluated with US. The statement emphasized that the combination of CT with US in preoperative lymph node evaluation is superior to the use of either modality alone.

In the Chinese Society of Clinical Oncology (CSCO) diagnosis and treatment guidelines for persistent/recurrent and metastatic differentiated thyroid cancer (version 2018) (56), when there are suspected local lesions, enhanced CT is juxtaposed as a level I–2A recommendation.

In the National Comprehensive Cancer Network (NCCN) guidelines (version 2018) (33), for papillary carcinoma or suspicious for papillary carcinoma, the use of CT with contrast was suggested for fixed, bulky, or substernal lesions. The NCCN guidelines (2020 V1) for diagnosing papillary carcinoma or suspected papillary carcinoma recommend the use of CT with contrast for locally advanced disease or vocal cord paresis.

The evidence provided in the above guidelines support the idea that enhanced CT is not a contraindication for patients with PTC. Moreover, CT examination can more accurately determine the extent of LNM, which is essential in the planning of surgical procedures.

In the current study, the patients were first suspected to have a malignant thyroid lesion with LNM by US, which was later confirmed as PTC by US-guided fine-needle aspiration biopsy (US-FNAB). DECT was performed to rule out or confirm the presence of LNM (45).

We used DECT for preoperative imaging instead of traditional enhanced CT due to its many advantages in comparison. The reasons for using DECT in the current study were as follows. First, its radiation dose (total dose-length product, DLP) was 5–6 times lower than that of ordinary enhanced CT (57). Second, DECT achieves a better image quality with significantly lower kVp and tube current. Third, DECT realizes multi-parameter imaging, such as single-energy images, energy spectrum curves, base material images, and the quantitative concentration values and effective atomic numbers of corresponding base materials.

The biggest advantage of DECT is that it not only shows morphological changes, but it also provides many quantitative indicators that could reflect the essential characteristics of lesions (58). The current study applied DECT to predict cervical metastatic lymph nodes with a diameter <0.5 cm in patients with PTC preoperatively, and to guide the planning of clinical procedures, which has not been reported before.

Preoperative DECT did not delay radioiodine ablation in patients with PTC

The NCCN guidelines (version 2018 and version 2020 V1) (19,20) clearly state that iodinated contrast is required for optimal cervical imaging using CT and that a delay in RAI treatment is not harmful to the patient.

Yeh *et al.* researched the content “Use of Iodinated Contrast and Impact on Subsequent Treatment” (9). The results showed that CT imaging of the neck was optimized by iodinated intravenous contrast. This advantage had to be balanced against the impact the iodine load would have in causing what was usually a minor delay in subsequent postoperative RAI ablation. After the administration of iodinated contrast, a waiting period of ≥ 1 month was recommended to allow urinary iodine levels to return to baseline levels before proceeding with RAI ablation (59). The CSCO expert consensus on the evaluation of ^{131}I before the treatment of differentiated thyroid cancer gave similar guidance. At present, there is no evidence to suggest that delays of this scale adversely affect thyroid cancer outcomes.

As we know, >90% of administered iodine is excreted in urine, and as the thyroid is the major reservoir of iodine in the body, iodine content should fall rapidly after total thyroidectomy, even in patients undergoing preoperative DECT (60). Furthermore, the recommendations against performing contrast-enhanced CT seem to be based on studies conducted in the past when lipophilic contrast agents were in use, which tend to be stored in adipose tissues for a long time. Currently the majority of centers use water-soluble ionic contrast agents (such as iohexol, which was used in our study), which are unlikely to be retained in extracellular fluids (60). Therefore, unless there is further iodine contamination, the urine iodine concentration (UIC) should soon revert to the previous equilibrium after DECT examination. Many studies have reported the time for UIC to normalize to be between 30 and 43 days (59–62). In addition, in routine practice, if the patients with PTC who come to our hospital for surgery need postoperative RAI therapy, the whole process “preoperative examination →

thyroidectomy → postoperative rehabilitation and discharge → appointment and preparation before RAI therapy → admission for RAI therapy” need to be completed. The entire process took ≥ 6 weeks without any delay, which was longer than required in the ATA guidelines. The 2015 ATA guidelines stated that postoperative RAI therapy should be routinely administered only to patients with high-risk differentiated thyroid cancer (DTC); it is not recommended for low-risk DTC and should only be considered for patients in the ATA intermediate-risk group (63). The majority of studies showed that the timing of post-thyroidectomy initial RAI therapy did not affect the overall survival or long-term outcomes of patients (64–68). Therefore, RAI administration may be safely planned according to the logistics of the local health administration and the individual patient (64).

In the current study, all participants who underwent DECT examination before surgery were given ≥ 1 month to recover before undergoing ^{131}I treatment after surgery, and the delay did not cause any harm according to our follow-up results.

Other inclusion criteria

Contrast agent enhancement of DECT depends on two factors. Firstly, injection-related factors, including contrast agent concentration and injection volume, contrast agent type, and saline injection; and secondly, patient-related factors, including cardiac output and body mass index (BMI) (69,70). Therefore, in the current study, we included participants with normal BMI (18.5–24.9 kg/m²). Overweight patients have decreased arterial enhancement. There is a negative linear relationship between body weight and the CT value of the common carotid artery (71). In addition, there is a moderate negative correlation between height and the CT value of the aorta (72). Since height is proportional to weight, the effect of height and weight on arterial strengthening should be in the same direction, and the effect of height should be weaker than that of weight. To eliminate the effect of different heights on weight and to enable a clearer comparison between groups in this study, patients with a normal BMI were selected.

Specific DECT diagnostic criteria of metastatic lymph nodes <0.5 cm in patients with PTC

Based on the previous CT diagnostic criteria for metastatic LNs, DECT diagnostic methods, and our clinical imaging

diagnosis experience, we summarized the following criteria for diagnosing LNM with a diameter <0.5 cm: strong or heterogeneous enhancement; micro-calcification; cystic degeneration or necrosis; extranodal extension; IC in the arterial phase ≥ 2.1 mg/mL; and IC in the venous phase ≥ 2.4 mg/mL (18,34,36) (Figure S7). Strong enhancement was considered to be similar to that of the pharyngeal mucosa. Fuzzy boundaries and/or invasion into adjacent tissues were considered to indicate extranodal extension (34).

DECT examination

Patients were instructed to hold their breath during eupnea before the horizontal scan in a transverse position. All patients were scanned craniocaudally in the supine position with the bilateral upper limbs placed on both sides, shoulders drooping maximally, and head slightly tilted. The longitudinal alignment of the positioning cursor was on the central sagittal plane of the cervicothoracic region. The orthotopic scanning was performed first, and then the scanning baseline and range were confirmed according to the scout view. The whole neck was scanned from the upper edge of the aortic arch to the lower edge of the submandibular gland, which covered the area of the thyroid and cervical lymph nodes.

The patient's heart rate was maintained at a normal level throughout the scan. After CT scanning, arterial phase and venous phase contrast-enhanced scanning was performed. The images were acquired in the dual-energy mode using the following parameters: tube current, 600 mA; helical thickness, 6 mm; helical pitch, 0.9; rotation speed, 0.28 s; detector width, 40 mm; collimation, 64 mm \times 0.6 mm. The scanning parameters were set according to the concept of as low as reasonably achievable for radiation protection. A fast rotation speed and a moderate helical pitch were chosen to obtain fast scanning speed and reduce motion artifacts of neck and radiation dose. For contrast-enhanced scanning, an iodinated nonionic contrast agent (iohexol; 350 mg/dL iodine, Somatom Definition Flash, Siemens Healthcare, Forchheim, Germany) was administered through the right elbow median vein by a dual-head injector. The dosage was 1 mL/kg with a flow rate of 3 mL/s, the total injection dose was 60–70 mL, followed by a bolus injection of 40 mL saline given at the same flow rate. The timing of arterial phase scanning was determined by automatic trigger technique. The scanning delay at the beginning of arterial phase scanning was 25 s. After the arterial scan had been completed, the scanning delay time of the venous scan was 20 s.

All the original CT data were reconstructed into contiguous axial images with a section thickness of 1 mm, a field of view (FOV) of 200 mm and a matrix of 512×512. The DECT data of arterial and venous phases were transferred to Siemens syngo.via workstation (Syngo DE, Siemens Healthcare, Forchheim, Germany) for analysis, the Liver VNC function keys for computer automatic processing, then the iodine maps were obtained.

Criteria for region of interest (ROI) selection in the current study

Firstly, under the premise of ensuring a clear image, we zoomed in to accurately measure the lesion. Secondly, we referred to the enhanced images of the arterial and the venous phases and the iodine maps of the arterial and the venous phases, and selected the layer that can clearly and completely display the largest cross-sectional area of the lymph node. Combining the sagittal, coronal, and axial images, the lymph node with the largest cross-sectional area for measurement was selected. The ROI was placed on the largest possible solid part, with attention paid to avoid cystic degeneration, necrosis, or calcification, and not involve adjacent blood vessels.

The division of cervical lymph nodes (focus on VIb)

In the American Joint Committee on Cancer (AJCC) 8th edition guidelines, the division of cervical lymph nodes plays an important role in clinical diagnosis and treatment. It meets the needs of the otolaryngology, head and neck surgery, and radiotherapy departments for the accurate positioning of cervical lymph nodes, as well as regulating the examination and facilitating academic exchange. However, it does not clearly define the parotid gland, cheeks, or scalp lymph node drainage, and some of the anatomical boundaries are not very accurate. In November 2013, the official journal of the European Society of Radiotherapy & Oncology (ESTRO)-Radiotherapy & Oncology (Green Skin Magazine) published a new cervical lymph node partition standard, which stated that according to the knowledge of anatomy, surgery, and imaging, the boundary should be accurately integrated into the axial CT image as much as possible. And the standard CT image was divided level VI into VIa and VIb (36). This is the most recently published cervical lymph node partition standard (*Table S2, Figures S8,S9*).

Result of consistency analysis

The inter-observer consistency analysis result for the ICC of the diameter diagnostic test between doctor A and doctor B was 0.959 ($P<0.001$) and the intra-observer consistency analysis result for the diameter was 0.957 ($P<0.001$) and 0.958 ($P<0.001$) for doctor A and doctor B, respectively. The inter-observer consistency analysis result for ICC of the IC in the arterial phase diagnostic test between doctor A and doctor B was 0.945 ($P<0.001$) and intra-observer consistency analysis result for the IC in the arterial phase was 0.957 ($P<0.001$), and 0.958 ($P<0.001$) in doctor A and doctor B, respectively. The inter-observer consistency analysis result for ICC of the IC in the venous phase diagnostic testing between doctor A and doctor B was 0.978 ($P<0.001$), and intra-observer consistency analysis result for the IC in the venous phase was 0.984 ($P<0.001$), and 0.984 ($P<0.001$), respectively.

References

43. Suh CH, Baek JH, Choi YJ, Lee JH. Performance of CT in the Preoperative Diagnosis of Cervical Lymph Node Metastasis in Patients with Papillary Thyroid Cancer: A Systematic Review and Meta-Analysis. *AJNR Am J Neuroradiol* 2017;38:154-61.
44. Lee Y, Kim JH, Baek JH, Jung SL, Park SW, Kim J, Yun TJ, Ha EJ, Lee KE, Kwon SY, Yang K S, Na DG. Value of CT added to ultrasonography for the diagnosis of lymph node metastasis in patients with thyroid cancer. *Head Neck* 2018;40:2137-48.
45. Cho SJ, Suh CH, Baek JH, Chung SR, Choi YJ, Lee JH. Diagnostic performance of CT in detection of metastatic cervical lymph nodes in patients with thyroid cancer: a systematic review and meta-analysis. *Eur Radiol* 2019;29:4635-47.
46. He M, Lin C, Yin L, Lin Y, Zhang S, Ma M. Value of Dual-Energy Computed Tomography for Diagnosing Cervical Lymph Node Metastasis in Patients With Papillary Thyroid Cancer. *J Comput Assist Tomogr* 2019;43:970-5.
47. Hong D, Lee S, Kim T, Baek JH, Lee YM, Chung KW, Sung TY, Kim N. Development of a personalized and realistic educational thyroid cancer phantom based on CT images: An evaluation of accuracy between three different 3D printers. *Comput Biol Med* 2019;113:103393.
48. Lee DH, Lee YH, Seo HS, Lee KY, Suh SI, Ryoo I, You SH, Kim B, Yang KS. Dual-energy CT iodine

- quantification for characterizing focal thyroid lesions. *Head Neck* 2019;41:1024-31.
49. Lee JH, Ha EJ, Kim JH. Application of deep learning to the diagnosis of cervical lymph node metastasis from thyroid cancer with CT. *Eur Radiol* 2019;29:5452-7.
 50. Yeom JA, Roh J, Jeong YJ, Lee JC, Kim HY, Suh YJ, Baik SK. Ultra-Low-Dose Neck CT With Low-Dose Contrast Material for Preoperative Staging of Thyroid Cancer: Image Quality and Diagnostic Performance. *AJR Am J Roentgenol* 2019;212:748-54.
 51. Debnam JM, Guha-Thakurta N, Sun J, Wei W, Zafereo ME, Cabanillas ME, Buisson NM, Schellingerhout D. Distinguishing Recurrent Thyroid Cancer from Residual Nonmalignant Thyroid Tissue Using Multiphasic Multidetector CT. *AJNR Am J Neuroradiol* 2020;41:844-51.
 52. Wei P, Jiang N, Ding J, Xiang J, Wang L, Wang H, Gu Y, Luo D, Han Z. The Diagnostic Role of Computed Tomography for ACR TI-RADS 4-5 Thyroid Nodules With Coarse Calcifications. *Front Oncol* 2020;10:911.
 53. Wei PY, Jiang ND, Xiang JJ, Xu CK, Ding JW, Wang HB, Luo DC, Han ZJ. Hounsfield Unit Values in ACR TI-RADS 4-5 Thyroid Nodules with Coarse Calcifications: An Important Imaging Feature Helpful for Diagnosis. *Cancer Manag Res* 2020;12:2711-7.
 54. Xing Z, Qiu Y, Yang Q, Yu Y, Liu J, Fei Y, Su A, Zhu J. Thyroid cancer neck lymph nodes metastasis: Meta-analysis of US and CT diagnosis. *Eur J Radiol* 2020;129:109103.
 55. Zhou Y, Su GY, Hu H, Ge YQ, Si Y, Shen MP, Xu XQ, Wu FY. Radiomics analysis of dual-energy CT-derived iodine maps for diagnosing metastatic cervical lymph nodes in patients with papillary thyroid cancer. *Eur Radiol* 2020;30:6251-62.
 56. Chinese Society of Clinical Oncology (CSCO) diagnosis and treatment guidelines for persistent/recurrent and metastatic differentiated thyroid cancer 2018 (English version). *Chin J Cancer Res* 2019;31:99-116.
 57. Agostini A, Mari A, Lanza C, Schicchi N, Borgheresi A, Maggi S, Giovagnoni A. Trends in radiation dose and image quality for pediatric patients with a multidetector CT and a third-generation dual-source dual-energy CT. *Radiol Med* 2019;124:745-52.
 58. Ren L, Rajendran K, McCollough CH, Yu L. Quantitative accuracy and dose efficiency of dual-contrast imaging using dual-energy CT: a phantom study. *Med Phy* 2020;47:441-56.
 59. Padovani RP, Kasamatsu TS, Nakabashi CC, Camacho CP, Andreoni DM, Malouf EZ, Marone MM, Maciel RM, Biscolla RP. One month is sufficient for urinary iodine to return to its baseline value after the use of water-soluble iodinated contrast agents in post-thyroidectomy patients requiring radioiodine therapy. *Thyroid* 2012;22:926-30.
 60. Mishra A, Pradhan PK, Gambhir S, Sabaretnam M, Gupta A, Babu S. Preoperative contrast-enhanced computerized tomography should not delay radioiodine ablation in differentiated thyroid carcinoma patients. *J Surg Res* 2015;193:731-7.
 61. Nimmons GL, Funk GF, Graham MM, Pagedar NA. Urinary iodine excretion after contrast computed tomography scan: implications for radioactive iodine use. *JAMA Otolaryngol Head Neck Surg* 2013;139:479-82.
 62. Sohn SY, Choi JH, Kim NK, Joung JY, Cho YY, Park SM, Bae JC, Lee SY, Chung JH, Kim SW. The impact of iodinated contrast agent administered during preoperative computed tomography scan on body iodine pool in patients with differentiated thyroid cancer preparing for radioactive iodine treatment. *Thyroid* 2014;24:872-7.
 63. Haugen BR, Alexander EK, Bible KC, Doherty GM, Mandel SJ, Nikiforov YE, Pacini F, Randolph GW, Sawka AM, Schlumberger M, Schuff KG, Sherman SI, Sosa JA, Steward DL, Tuttle RM, Wartofsky L. 2015 American Thyroid Association Management Guidelines for Adult Patients with Thyroid Nodules and Differentiated Thyroid Cancer: The American Thyroid Association Guidelines Task Force on Thyroid Nodules and Differentiated Thyroid Cancer. *Thyroid* 2016;26:1-133.
 64. Suman P, Wang CH, Moo-Young TA, Prinz RA, DJ W. Timing of radioactive iodine administration does not influence outcomes in patients with differentiated thyroid carcinoma. *Thyroid* 2016;26:1623-9.
 65. Tsirona S, Vlassopoulou V, Tzanela M, Rondogianni P, Ioannidis G, Vassilopoulos C, Botoula E, Trivizas P, Datsaris I, Tsagarakis S. Impact of early vs late postoperative radioiodine remnant ablation on final outcome in patients with low-risk well-differentiated thyroid cancer. *Clin Endocrinol (Oxf)* 2014;80:459-63.
 66. Krajewska J, Jarzab M, Kukulka A, Czarniecka A, Roskosz J, Puch Z, Wygoda Z, Paliczka-Cieslik E, Kropinska A, Krol A, Handkiewicz-Junak D, Jarzab B. Postoperative Radioiodine Treatment within 9 Months from Diagnosis Significantly Reduces the Risk of Relapse in Low-Risk Differentiated Thyroid Carcinoma. *Nucl Med Mol Imaging* 2019;53:320-7.
 67. Kim M, Han M, Jeon MJ, Kim WG, Kim IJ, Ryu JS, Kim WB, Shong YK, Kim TY, Kim BH. Impact of delayed

- radioiodine therapy in intermediate-/high-risk papillary thyroid carcinoma. *Clin Endocrinol (Oxf)* 2019;91:449-55.
68. Suman P, Wang CH, Abadin SS, Block R, Raghavan V, Moo-Young TA, Prinz RA, Winchester DJ. Timing of Radioactive Iodine Therapy Does Not Impact Overall Survival in High-Risk Papillary Thyroid Carcinoma. *Endocr Pract* 2016;22:822-31.
 69. Schoellnast H, Deutschmann HA, Berghold A, Fritz GA, Schaffler GJ, Tillich M. MDCT angiography of the pulmonary arteries: influence of body weight, body mass index, and scan length on arterial enhancement at different iodine flow rates. *AJR Am J Roentgenol* 2006;187:1074-8.
 70. Bae KT, Seeck BA, Hildebolt CF, Tao C, Zhu F, Kanematsu M, Woodard PK. Contrast enhancement in cardiovascular MDCT: effect of body weight, height, body surface area, body mass index, and obesity. *AJR Am J Roentgenol* 2008;190:777-84.
 71. Bae KT, Tao C, Gurel S, Hong C, Zhu F, Gebke TA, Milite M, Hildebolt CF. Effect of patient weight and scanning duration on contrast enhancement during pulmonary multidetector CT angiography. *Radiology* 2007;242:582-9.
 72. Awai K, Hori S. Effect of contrast injection protocol with dose tailored to patient weight and fixed injection duration on aortic and hepatic enhancement at multidetector-row helical CT. *Eur Radiol* 2003;13:2155-60.
 73. Gregoire V, Ang K, Budach W, Grau C, Hamoir M, Langendijk JA, Lee A, Le QT, Maingon P, Nutting C, O'Sullivan B, Porceddu SV, Lengele B. Delineation of the neck node levels for head and neck tumors: a 2013 update. DAHANCA, EORTC, HKNPCSG, NCIC CTG, NCRI, RTOG, TROG consensus guidelines. *Radiother Oncol* 2014;110:172-81.